DEPARTMENT OF EXPERIMENTAL PHYSICS
LABORATORY OF BIOPHYSICS
FACULTY OF SCIENCE
PALACKÝ UNIVERSITY IN OLOMOUC
OLOMOUC, CZECH REPUBLIC

INTERACTION OF SMALL ORGANIC MOLECULES WITH THE SODIUM PUMP

MARIKA JANOVSKÁ

Olomouc 2010

ACKNOWLEDGEMENT

ABSTRACT

The balance between concentrations of Na and K ions across cell membranes is a fundamental property which is utilized in numerous physiological processes. The establishment of the concentration gradient is carried out by Na^+/K^+-ATPase (also called sodium pump), which was first identified in the late 1950s in Aarhus by the Danish scientist J. C. Skou. Na^+/K^+-ATPase is heterodimeric membrane protein consisting of three subunits (α, β, and γ). It belongs to the family of P-type ATPases, which use energy for ion translocation through the cell membrane from ATP hydrolysis and the pumping process involves a phosphorylated intermediate. For the proper function of Na^+/K^+-ATPase, Mg^{2+} cations must be present in cytoplasm as an essential cofactor (Skou 1960). Because of importance of Na^+/K^+-ATPase in many physiological processes, inhibition of its activity can cause serious illnesses in humans and can be the main reason for the toxicological effects of numerous drugs. Recently, high-resolution crystal structure of Na^+/K^+-ATPase was described (Morth et al. 2007, Shinoda et al. 2009).

Alkaloids are one of the largest groups of plant secondary metabolites, and they are interesting for their biological activities. Sanguinarine (SG), the benzo[c]phenanthridine alkaloid, exhibits multiple biological effects, in particular antimicrobial and antiinflammatory activities, for which it is used in dental hygiene products and feed additives. On the other hand, SG is linked to toxic effects on humans such as the formation of leukoplakia and the syndrome termed epidemic dropsy. From the chemical point of view, in a solution, there is an acido-basic equilibrium between the cationic- (SG^+) and pseudobase (SGOH) forms of SG, and in the gastrointestinal tract, SG is converted to biologically inactive dihydrosanguinarine (DHSG). All the forms exhibit fluorescence. Na^+/K^+-ATPase has been proposed as a possible target of these alkaloids.

We combined the steady-state and time-resolved fluorescence techniques to distinguish fluorescence properties of the individual SG forms and to study their changes expected upon the interactions with proteins. In the study, where the SG was incubated with Na^+/K^+-ATPase, evaluation of the SG fluorescence characteristics provided valuable information about the structural details of the SG/enzyme interactions. Moreover, we were able to identify SG^+-binding site on Na^+/K^+-ATPase.

Large cytoplasmic loop of Na^+/K^+-ATPase located between fourth and fifth transmembrane helices of its α-subunit (C45) contains both phosphorylation and ATP-binding sites. It was

shown that it retains its tertiary structure even when separated from the rest of the protein, and can thus still bind ATP (Kubala et al. 2003). We used methods of intristic tryptophan fluorescence measurement and molecular dynamic simulations to study conformational changes of isolated large cytoplasmic loop of Na^+/K^+-ATPase (C45) induced by cytoplasmic ligand binding (i. e., Mg^{2+} and/or ATP). Our experiments revealed that binding of ATP in the absence of Mg^{2+} induced the open C45 conformation, while presence of Mg^{2+} stabilized the closed conformation. Moreover, we introduced a novel method for monitoring changes in electrostatic surface potential (ESP) caused by natural cytoplasmic ligands binding. Our data indicate that the effect of the ligand binding is not restricted only to the close environment of the binding site and that the information is in fact transmitted also to the distal parts of the molecule.

LIST OF PUBLICATIONS

This thesis is based on the following papers, which are referred to in the text by their Roman numerals I-V.

I.   **Janovská M**, Kubala M, Šimánek V, Ulrichová J (2009) Fluorescence of Sanguinarine: fundamental characteristics and analysis of interconversion between various forms. *Anal. Bioanal. Chem. 395, 235-240*

II.   **Janovská M**, Kubala M, Šimánek V, Ulrichová J (2010) Fluorescence of Sanguinarine: Spectral changes on interaction with amino acids. *Phys. Chem. Chem. Phys., Submitted*

III.   **Janovská M**, Kubala M, Šimánek V, Ulrichová J (2010) Interaction of sanguinarine and its dihydroderivative with the Na^+/K^+-ATPase. Complex view on the old problem. *Toxicol. Lett. 196, 56-59*

IV.   Gryčová L, Sklenovský P, Lánský Z, **Janovská M**, Otyepka M, Amler E, Teisinger J, Kubala M (2009) ATP and magnesium drive conformational changes of the Na^+/K^+-ATPase cytoplasmic headpiece. *Biochim. Biophys. Acta 1788, 1081-1091*

V.   Kubala M, Gryčová L, Lánský Z, Sklenovský P, **Janovská M**, Otyepka M, Teisinger J (2009) Changes in the electrostatic surface potential of the Na^+/K^+-ATPase cytoplasmic headpiece induced by the cytoplasmic ligand(s) binding. *Biophys. J. 97(6), 1756-1764*

CONTENTS

LIST OF ABBREVIATIONS

Amino acids

A	Ala	alanine	I	Ile	isoleucine	R	Arg	arginine
C	Cys	cysteine	K	Lys	lysine	S	Ser	serine
D	Asp	aspartic acid	L	Leu	leucine	T	Thr	threonine
E	Glu	glutamic acid	M	Met	methionine	V	Val	valine
F	Phe	phenylalanine	N	Asn	asparagine	W	Trp	tryptophan
G	Gly	glycine	P	Pro	proline	Y	Tyr	tyrosine
H	His	histidine	Q	Gln	glutamine			

The number by the amino acid abbreviation gives its position in the sequence from the N-terminus, e.g.:

Arg^{979} Arginine at the position 979

ADP   Adenosine diphosphate

ATP   Adenosine triphosphate

αMx   xth transmembrane helix of Na$^+$/K$^+$-ATPase α-subunit (x-number)

βM   Transmembrane helix of Na$^+$/K$^+$-ATPase β-subunit

Ca^{2+}-ATPase   Ca^{2+}-adenosinetriphosphatase

C45   Cytoplasmic loop of Na$^+$/K$^+$-ATPase located between fourth and fifth transmembrane helices of its α-subunit

DAS   Decay-associated spectra

DHSG   Dihydrosanguinarine

DMSO   Dimethylsulfoxide

DTT   Dithiothreitol

EDTA   Ethylenediaminetetraacetic acid

ESP   Electrostatic surface potential

E78   Extracellular loop of Na$^+$/K$^+$-ATPase located between seventh and eighth transmembrane helices of its α-subunit

γM   Transmembrane helix of Na$^+$/K$^+$-ATPase γ-subunit

H^+/K^+-ATPase	H^+/K^+- adenosinetriphosphatase
IRF	Instrument Response Function
ISOM	Medium for cell cultivation named after Harriet C. Isom
K_D	Dissociation constant
K_{sv}	Stern-Volmer quenching constant
LED	Light Emitting Diode
Mat-8	Mammary tumor marker
MD	Molecular dynamic (simulations)
NADH	Nicotinamide adenine dinucleotide (reduced form)
Na^+/K^+-ATPase	Na^+/K^+- adenosinetriphosphatase
PBS	Phosphate buffer saline
PLM	Phospholemman
QBA	Quarternary benzo[c]phenanthridine alkaloid
SDS-PAGE	Polyacrylamide gel electrophoresis under denaturing conditions
SERCA	Sarco(endo)plasmic Ca^{2+}-ATPase
SG	Sanguinarine
SG^+	Quarternary cation of sanguinarine
SGOH	Pseudobase form of sanguinarine
TCSPC	Time-correlated single photon counting
TL	Tryptophanless (construct)
TNP-ATP	2′,3′-O-(2,4,6- trinitrophenyl) adenosine 5′-triphosphate
WT	Wild type sequence

1 INTRODUCTION

1.1 P-type ATPase superfamily

Generally, Na^+/K^+-ATPase, also called sodium pump, belongs to the group of ion-motive ATPases. Ion-motive ATPases are conventionally divided into three distinct families, V-, F-, and P-type ATPases (Pedersen and Carafoli 1987a).

The V-type (vacuolar-type) ATPases are multi-subunit electrogenic proton pumps. They comprise a closely related family that reside in the membranes of acidic organelles in eukaryotic cells. They are critical for receptor recycling pathways by adicifying endocytotic vesicles and promoting receptor-ligand dissociation (Kaplan 2002). V-type ATPases are also found in epithelia of vertebrate kidney, lepidopteran midgut epithelium and insect Malpighian tubules (Kaplan 2002).

F-type ATPases are proton ATPases found in the inner mitochondrial membrane, the chloroplast thylakoid membrane, and the bacterial plasma membrane (Pedersen and Carafoli 1987b). In mitochondria and chloroplasts under physiological conditions, the enzyme works exclusively as an ATP-synthase, driven by an electrochemical H^+ gradient. Bacterial F-type ATPases also hydrolyse ATP and expel H^+ from the cell (Kaplan 2002).

P-type transport ATPases comprise an important family of homologous enzymes of eucaryotic and procaryotic origin which are involved in the active pumping of cations across cell membranes. The P-type ATPase gene family of ion pumps is widely distributed in fungi, Protozoa, plants, and animals. P-type (or E_1E_2 type) ATPases are so called because the enzyme works via a covalent, phosphorylated intermediate, thus the formation of the acyl phosphate intermediate is a hallmark of the members of the P-type ATPase family. The 7 amino acid motif beginning with this aspartate can be written as D-K-T-G-T-[LIVM]-[TIS] and defines membership in P-type ATPase family (Kaplan 2002).

P-type ATPases pump a variety of charged substrates such as K^+, Na^+, H^+, Mg^{2+}, Ca^{2+}, Cu^{2+}, Cd^{2+} and phospholipids. In each P-type ATPases, eight conserved segments comprising a total of 265 amino acids can be identified (Palmgren and Axelsen 1998b).

The conserved domains are situated in the small cytoplasmic loop between transmembrane segments 2 and 3 (4 and 5 in type IB ATPases; Fig. 1), the fourth transmembrane segment (6 in type IB), and the large cytoplasmic loop between transmembrane segments 4 and 5 (6 and 7 in type IB; Fig. 1). These parts of the polypeptide are believed to be involved in

communication between ATP hydrolysis and conformational change (the energy transduction domain), in ion binding and in ATP binding, respectively, features that are common between all P-type ATPases (Møller et al. 1996). In Na^+/K^+- and H^+/K^+-ATPases, the fourth transmembrane segments in addition contain specific targeting information (Palmgren and Axelsen 1998a).
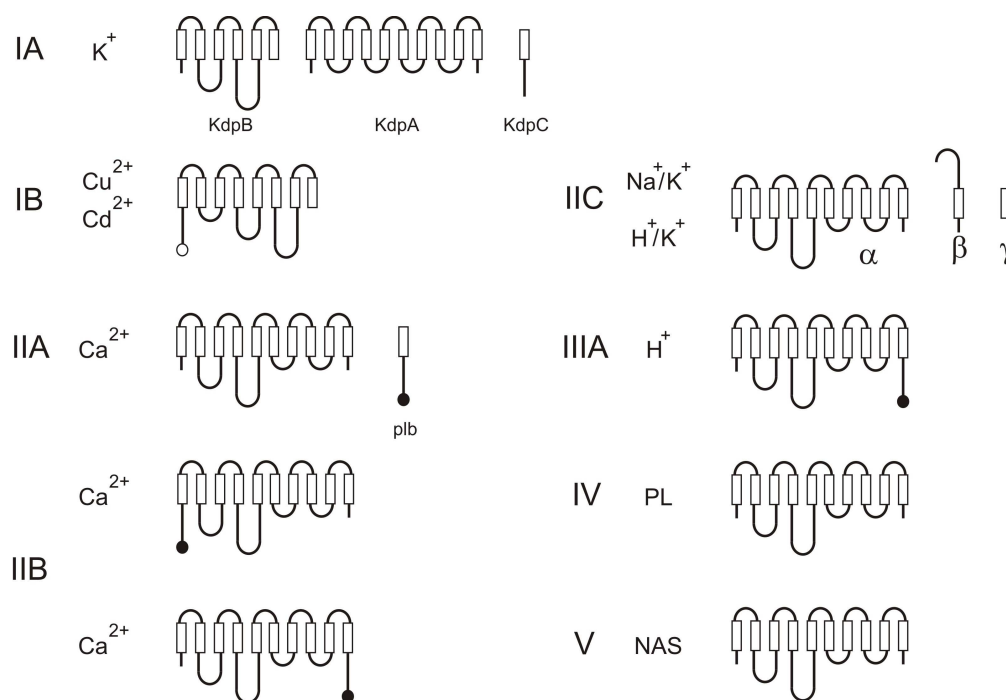
Figure 1 Overview of the P-type ATPases superfamily. Families are designated by Roman numerals on the left followed by the name of the transported ion. Boxes indicate transmembrane segments; Filled circles, inhibitory sequences; Open circles, heavy metal binding sites. Abbreviations are: PL, phospholipids; NAS, no assigned specificity; plb, phospholamban. On each structure, extracellular side is located up and cytoplasmic side is located below.

1.2 Na^+/K^+-ATPase

Na^+/K^+-ATPase is the largest protein complex in the family of P-type pumps. The Na^+/K^+-ATPase or sodium pump is the protein responsible for the active transport or pumping of Na^+ and K^+ ions across the plasma membranes of most higher eukaryotes. The presence of cell

membranes with ATPase activity that was stimulated by the simultaneous presence of Na^+ and K^+ ions and was specifically inhibited by cardiac glycosides was discovered more than forty years ago and was recognized in 1997 with the shared award of the Nobel Prize in Chemistry to Jens C. Skou (Kaplan 2002).

The Na^+/K^+-ATPase (Fig. 2) is essential for all mammalian cells. At rest, it consumes 20-30% of ATP production to actively transport Na^+ and K^+ ions. The overall stoichiometry of the reaction is three Na^+ ions transported out of the cell and two K^+ ions into the cell for each ATP hydrolyzed (Xu 2005). The Na^+ and K^+ gradients are required for maintaining membrane potentials, cell volume and secondary active transport of other solutes, e. g. , the transcellular transport processes in intestine, glands and kidney (Jörgensen et al. 2003).
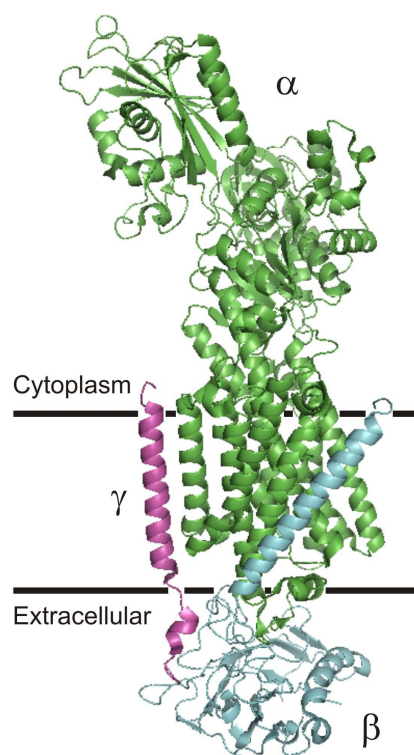
Figure 2 Architecture of the Na^+/K^+-ATPase $\alpha\beta\gamma$ complex (PDB entry 2ZXE). The α-, β-, and γ-subunits are coloured green, blue and violet, respectively. Helices are represented by spirales and β-strands by arrows.

The Na^+/K^+-ATPase and its closely related cousin, the gastric H^+/K^+-ATPase, are the only members of the P-type ATPase family composed of more than one subunit. These are heterodimeric proteins consisting of an α- and β-subunit present in 1:1 stoichiometry (Kaplan 2002). Four α- and three β-isoforms of Na^+/K^+-ATPase subunit have been identified, which

show a tissue-specific expression and can potentially form 12 different Na^+/K^+-ATPase isozymes with distinct transport and pharmacological properties (Blanco and Mercer 1998, Geering 2006). α- and β-subunit of Na^+/K^+-ATPase may also be coexpressed with small ion transport regulators of the FXYD family (Sweadner and Rael 2000).

First X-ray crystal structure of pig renal Na^+/K^+-ATPase αβγ complex (Fig. 2), with bound K^+/Rb^+ counterions, in 3.5 Å resolution was presented by Morth et al. (2007). Two years later, Shinoda et al. (2009) published crystal structure of Na^+/K^+-ATPase in 2.5 Å resolution, which was isolated from shark rectal glands.

1.2.1 α-subunit

The Na^+/K^+-ATPase α-subunit is composed of ~ 1000 amino acid residues (Morth et al. 2007). It has a molecular mass of about 110 kDa, and four distinct isoforms have been identified (Kaplan 2002).

An outline of the α-subunit is shown in the Fig. 3. Extracellular loops are short (with exception of E78 loop), and there are three main intracellular structures. These are a large central loop between αM4 and αM5 (C45), composed of about 430 amino acid residues, a long N-terminal tail of about 90 amino acid residues, and an intracellular loop of about 120 residues between αM2 and αM3 (C23).
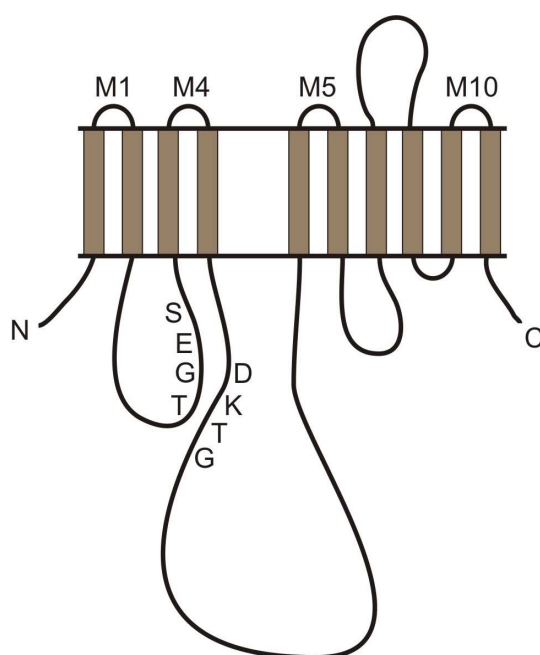
Figure 3 An outline of the α-subunit.

In the terminology of Toyoshima´s SERCA high-resolution structure, they form the N or nucleotide-binding domain, the P or phospohorylation domain, and the A or actuator domain (Fig. 4) (Toyoshima et al. 2000). The N and P domains are formed by the C45 loop, the A domain is formed by the amino-terminal tail and the C23 loop (Shinoda et al. 2009).
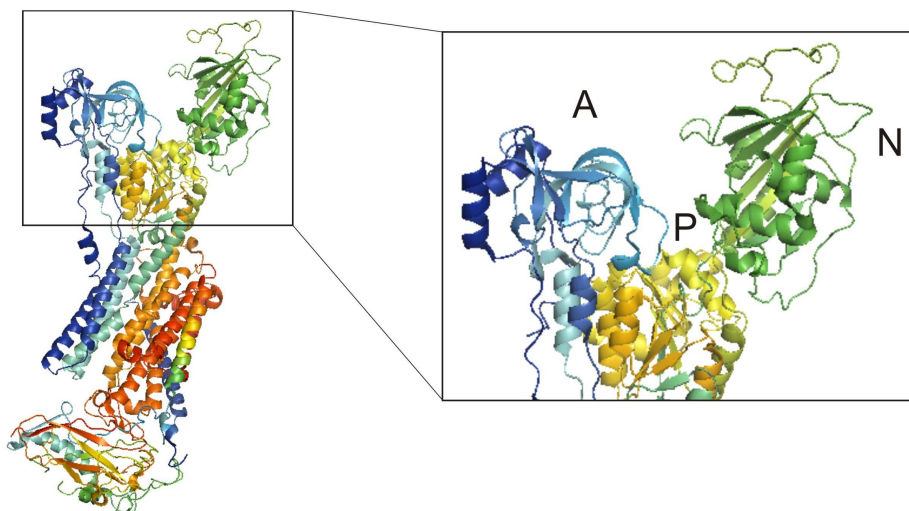
Figure 4 Alignment of Na^+/K^+-ATPase cytoplasmic domains (PDB entry 2ZXE). Na^+/K^+-ATPase is displayed in spectrum colors from N-terminus (blue) to C-terminus (dark yellow). A (actuator), N (nucleotide binding), and P (phosporylation) domains are coloured blue, green, and yellow, respectively. Helices are represented by spirales and β-strands by arrows.

Two cation-binding sites (common to both sodium and potassium) are localized in the transmembrane domain. They are formed by the residues of the transmembrane helices αM4, αM5, αM6 and αM8. αM4 and αM6 helices of Na^+/K^+-ATPase are unwound in the middle, thereby making space for the ions, and αM1 shows a characteristic ~90° kink near the cytoplasmic surface of the membrane, where it comes into contact with αM3. This contact point may function as a pivot for movement of αM1 in connection with ion binding (Morth et al. 2007). The segment of αM7 located near the cytoplasmic surface has a distinct kink of ~18˚, which appears to have central importance in K^+ binding. Moreover, helices αM7-αM10 appear to have a dynamic role in Na^+/K^+-ATPase and might be used to change the position of the cytoplasmic domain of the β-subunit (Shinoda et al. 2009).

Four different isoforms of α-subunit have been found in humans (Lingrel et al. 2007). Each can associate with a β-subunit in 1:1 stoichiometry to form a minimal functional unit. The

corresponding isoforms in human and rat are more similar (> 97% identity) than different isoforms in the same species (86 – 87%) (Grishin et al. 1994).

Morth et al. (2009) visualized differences between the three major human isoforms α_1, α_2, and α_3. It was shown that there are very few isoform differences in the transmembrane region, suggesting that these areas are conserved and important for function and the basic transport mechanism and stability. In opposite, there are many more differences at surface-exposed regions of the A- and N-domains, reflecting, probably, isoform specific interactions with other cellular components.

1.2.2 *β-subunit*

Na^+/K^+-ATPase and H^+/K^+-ATPase are the only members of the P-type ATPase family known to contain a β-subunit.

The β-subunit is a type II transmembrane glycoprotein with ~300 amino acids residues consisting of a cytoplasmic amino-terminal domain of about 40 residues, a single membrane spanning segment, and a larger extracellular carboxyl-terminal domain comprising about 240 amino acid residues (Laughery et al. 2003) (Fig. 5). The extracellular domain has three *N*-linked glycosylation sites, which are conserved throughout all β subunit isoforms of various species (Dempski et al. 2005), and in addition three S-S bridges in the extracellular domain (Kaplan 2002). The disulfides are required for targeting to the plasma membrane and are highly resistant to reduction (Laughery et al. 2003). The β-subunit has an overall apparent molecular mass of 55 kDa, and three isoforms have been reported. All β isoforms are heavily glycosylated. The β_1-isoform from mammals has three *N*-linked glycosylation sites. The putative *N*-linked glycosylation sites for the β_2-isoform vary depending on the species (Blanco and Mercer 1998).

According to the results of Dempski et al. (2006), transmembrane helix of β-subunit is adjacent to the αM9-αM8-αM10 pocket. Shinoda et al. (2009) described that the transmembrane helix of the β-subunit runs rather detached from those of the α-subunit and is inclined by ~32° from the membrane normal, nearly parallel to αM7. It was shown that βM is closest to αM7, and approaches αM10 near the extracellular end (Morth et al. 2007).
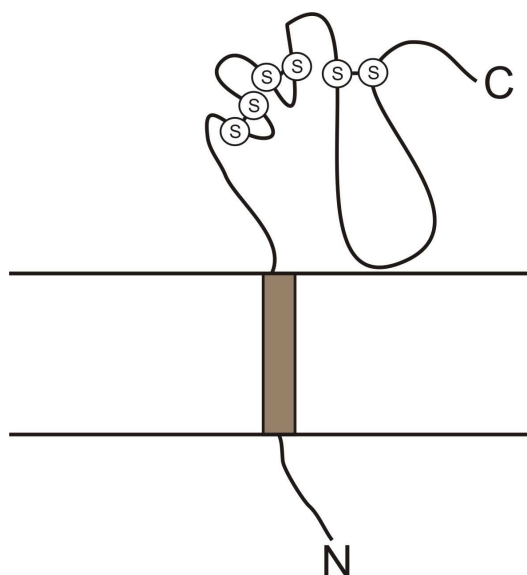
Figure 5 An outline of the β-subunit.

Geering (2001) reported results, which establish that β-subunit has two main functions. Of fundamental importance is the role of the β-subunit as a specific chaperone, which assists in the correct membrane insertion of the newly synthesized Na^+/K^+-ATPase and H^+/K^+-ATPase α-subunits and, hence, in their structural and functional maturation. In addition, association of the β-subunit determines some of the intrinsic transport properties of Na^+/K^+- and H^+/K^+-ATPases, it modulates cation sensitivity of the pump (Dempski et al. 2005). Morth et al. (2007) described clear indication that the β-subunit completely covers the extracellular αM5-αM6 and αM7-αM8 loops as a lid, which may relate to the essential role of the β-subunit in K^+ occlusion. According to the results of Shinoda et. al (2009), there is complex interactions between the β- and α-subunit, created with salt-bridges between βArg[183], αGlu[899] and βLys[250], which implicate the β-subunit modulation of cation transport.

It was shown that extracellular domain of the β-subunit undergoes a conformation rearrangement during E_1 to E_2 transition (Dempski et al. 2006). α- and β-subunits are moving towards during conformation transition, moreover, these interactions are dynamic. There is a structural re-arrangement between the extracellular transmembrane region of the β-subunit and both the αM3-αM4 and αM5-αM6 regions during ion translocation.

1.2.3 γ-subunit

The γ-subunit of Na^+/K^+-ATPase is a member of the family of FXYD proteins. FXYD proteins are simple transmembrane proteins named after the invariant extracellular motif FXYD. In mammals, the FXYD protein family contains seven members (Geering 2005). Specific association with the Na^+/K^+-ATPase and effects on the pump function have been reported for FXYD1 (also known as phospholemman, or PLM), FXYD2 (also known as the γ-subunit of Na^+/K^+-ATPase), FXYD3 (also know as Mat-8), FXYD4 (also known as corticosteroid hormone-induced factor, or CHIF), FXYD7, and PLM-like protein from shark rectal gland (PLMS) (Garty and Karlish 2006).

FXYD proteins are tissue-specific auxilary subunit of Na^+/K^+-ATPase which regulate its activity in agreement with the physiological requirements of the tissue in which they are expressed (Geering 2005). These proteins are short polypeptides (>100 amino acids) with a single transmembrane segment and with or without a signal peptide (Garty and Karlish 2006). Transmembrane segment of γ-subunit has approximately 30 amino acids with mostly α-helical structure. Extracellular part of the γ-subunit, containing FXYD motif (Fig. 6), moves in between α- and β-subunits, where it may contact with the β-subunit. It is close to the αM9, where Phe^{949}, Glu^{953}, Leu^{957} and Phe^{960} are within interaction distance of γM (Morth et al. 2007). On the other side, two conserved Gly residues of γM play important role in the interaction with αM9, particularly Gly^{34} (Shinoda et al. 2009).
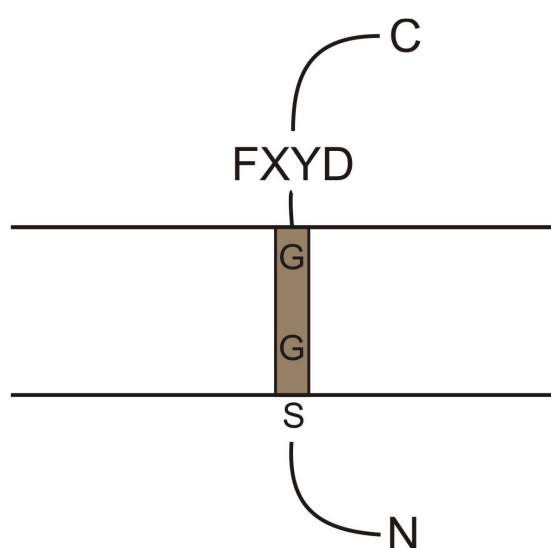
Figure 6 An outline of γ-subunit with indications of the positions of conserved amino acid residues.

1.2.4 Active transport and ATP hydrolysis

Basically, the reaction mechanism can be formulated in terms of a 4 step scheme: $E_1 \rightarrow E_1P$ $\rightarrow E_2P \rightarrow E_2 \rightarrow E_1$. This scheme is generally referred to as the Post-Albers scheme in the case of Na^+/K^+-ATPase (Albers and Siegel 1967, Post et al. 1972).

The Na^+/K^+-ATPase couples ATP hydrolysis to the active transport of three Na^+ ions out of and two K^+ ions into the cell in a ping-pong sequence, while alternating between two cation complexes $E_1P[3Na]$ and $E_2[2K]$ (Jörgensen and Andersen 1988). In the model of the reaction cycle (Fig. 7) relatively large E_1-E_2 conformational changes in the α-subunit mediate long-range interactions between the ATP site and the cation sites in the membrane domain (Lutsenko and Kaplan 1995). In the initial step, binding of ATP with low apparent affinity ($K_m \approx 0,2$-$0,4$ mM) to the $E_2[2K]$ conformation accelerates the $E_2[2K]$-$E_1[2K]$ transition with release of K^+ at the cytoplasmic surface. ATP is bound with high affinity in the E_1 conformation ($K_D \approx 300$-100 nM) (Jörgensen and Andersen 1988) and the increase in binding energy of ATP associated with the $E_2[2K]$-$E_1[2K]$ conformational transition constitues the driving force for transport of K^+ across the membrane. The next energy transducing steps are the Na-dependent transfer of γ-phosphate from ATP to an acyl bond at Asp^{369} of the α-subunit and isomerization between the occluded $E_1P[3Na]$ and $E_2P[2Na]$ forms in coupling with reorientation of cation sites and release of Na^+ ions at the extracellular surface (Jörgensen and Pedersen 2000). Na^+/K^+-ATPase also exhibits ATP-K^+ antagonism because the two high affinity ligands stabilize alternative conformations, $E_2[2K]$ with tightly bound K^+ ions or E_1ATP with a preference for binding of Na^+ (Fig. 7). The ATP and cation binding assays can therefore be exploited in estimation of the poise of the equilibrium between the E_1 and E_2 conformations of the protein and in determination of the affinities for K^+. Affinities for Na^+ or Mg^{2+} binding can be assayed in the $E_1P[3Na]$ form using oligomycin to stabilize the phosphorylated complex (Pedersen et al. 2000). The E_2P form can be stabilized in the ouabain complex for estimates of the affinities for binding of Mg^{2+} or inorganic phosphate (Jörgensen and Pedersen 2001). High affinity binding of Rb^+ and Tl^+ can be assayed in purified renal Na^+/K^+-ATPase or in recombinant yeast enzyme at equilibrium with dissociation constants K_D = 7-9 µM (Pedersen et al. 2000).
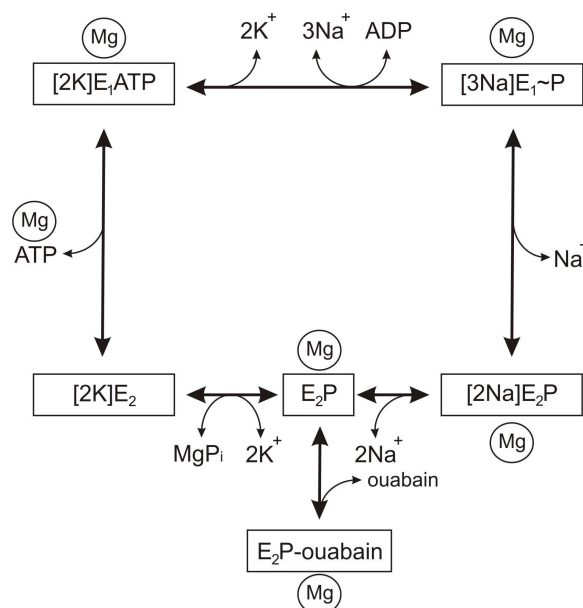
Figure 7 Scheme of $E_1 \rightarrow E_2$ reaction cycle of Na^+/K^+-ATPase with ping-pong sequential cation translocation.

A characteristic feature of E_1-E_2 transitions is that the active site alters its size owing to domain association and dissociation and its inclination through tilting or rotation of the P domain. It was described, that relationship between the N and P domains does not change much during the reaction, but association and dissociation of the A domain is a prominent feature (Toyoshima et al. 2000, Xu et al. 2002).

1.2.5 Large cytoplasmic segment C45

Large cytoplasmic loop, located between helices $\alpha M4$ and $\alpha M5$ (C45, Fig. 8), which is composed of about 420 amino acid residues (Lys^{354}-Lys^{773}) with molecular weight about 48kDa, plays a key role in the enzyme function. The loop consists of two well-separated domains. The P-domain comprises the phosphorylation site and the N-domain contains the ATP-binding site.

C45 loop contains four of the most highly conserved P-type ATPase sequences, including the sequence Asp-Lys-Thr-Gly-Ser/Thr (Fig. 8), which contains an invariant aspartate residue (Asp^{369}) that is phosphorylated by ATP as part of the catalytic mechanism of these proteins. Transfer of the γ-phosphoryl group from ATP to the proteins is an essential step in the catalysis of ion transport by all P-type ion pumps.
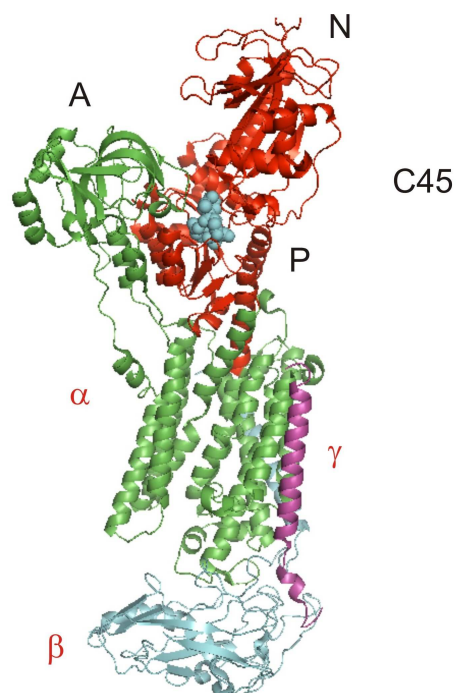
Figure 8 Location of C45 loop (coloured red) within the $\alpha\beta\gamma$ complex of Na$^+$/K$^+$-ATPase (PDB entry 2ZXE). Conserved sequence Asp-Lys-Thr-Gly-Ser/Thr is shown as cyan spheres. The α-, β-, and γ-subunits are coloured green, blue and violet, respectively. Helices are represented by spirales and β-strands by arrows. Actuator, nucleotide binding, and phophorylation domains are signed A, N and P, respectively.

The E$_1$[Na] and E$_2$[K]-conformations of Na$^+$/K$^+$-ATPase are intimately connected to the E$_1$ATP and E$_2$ATP sites with different affinities for ATP. E$_1$ATP site is considered as state with high affinity for ATP with K_D value approximately 1 μM and E$_2$ATP site is considered as state with low affinity for ATP with K_D value approximately 200 μM (Lingrel and Kuntzweiler 1994).

It was shown that in site-directed mutagenesis experiments with C45 loop that there are eight amino acids analogues involved in ATP binding – Lys^{480}, Lys^{501}, Gly^{502}, Cys^{549}, Phe^{475}, Gln^{482}, Phe^{548} and Glu^{446} (Kubala et al. 2002, Kubala et al. 2003b). Ser^{445} is also located close to the ATP-binding site, although it does not participate in binding (Kubala et al. 2002).

Pedersen et al. (2000) observed role of highly conserved segment ^{708}TGDGVNDSPALKK^{720} of isolated large cytoplasmic loop C45 in binding of Mg^{2+} and ATP. They described, that Asp^{710} contributes to coordination of Mg^{2+} during transfer of γ-phosphate to Asp^{369} of the Mg.E$_1$P[3Na] complex and Asn^{710} is involved in these processes. In contrast, Asp^{710} and

Asp^{713} do not contribute to Mg^{2+} binding in E_2P.ouabain complex. It means that during transition from E_1P to E_2P complex there is a shift of Mg^{2+} away from Asp^{710} and Asn^{713}.

It has been shown that this loop retains its tertiary structure even when separated form the rest of the protein (Tran and Farley 1999), and can be expressed in bacterial cells with histidine tag (Gatto et al. 1998).

It has been shown, from steady-state experiment with TNP-ATP and from dynamic experiments, that this large cytoplasmic loop binds ATP (Obšil et al. 1998, Kubala et al. 2003). However, Kubala et al. (2003) described that when interpreting the results of assays performed with TNP-ATP, it is necessary to take into acount the fact that its interaction with proteins may not mimic perfectly the behaviour of pure ATP.

1.2.6 Physiological role of Na⁺/K⁺-ATPase

As mentioned above, the Na^+/K^+-ATPase is an integral membrane protein that transports Na^+ and K^+ across the plasma membrane of almost all animal cells and couples this work to the hydrolysis of the terminal phosphate bond of ATP. A significant fraction (up to $\approx 30\%$) of the ATP generated by cell metabolism is dedicated to their active transport process (Kaplan 2002).

In general, the electrical gradient created by the sodium pump is essential for the excitable activity of muscle and nerve tissue, and the inwardly directed Na gradient maintaned by the sodium pump is used in most cells and organs to drive the uptake and accumulation of a wide range of essential nutrients and cellular substrates and to reduce cell calcium and proton concentration.

The concentration of Na^+/K^+-ATPase in tissues varies largely with around a 160,000 fold diference between the lowest (erythrocytes) and the highest (brain cortex) concentrations. The vascular smooth muscle is in the lower range of the spectrum with very limited concentration of pumps (400,000 – 700,000 pumps/cell); ~ 100 times lower than that seen on heart or skeletal muscle (Köksoy 2002).

Isoforms for the α- and β-subunits of Na^+/K^+-ATPase have been identified, all exhibiting unique tissue-end developmental expression patterns, and specific functional roles for each are now beginning to be defined.

Three isoforms of the β-subunit exist: β_1, β_2 and β_3. The α-subunit has four isoforms, α_1, α_2, α_3 and α_4. While the α_1-isoform is expressed ubiquitously, the α_2-isoform is present largely in

skeletal muscle, heart, brain, adipocytes, vascular smooth muscle, and eye, as well as a number of other tissues. The α_3-isoform is found almost exclusively in neurons and ovaries, but also occurs in white blood cells and heart of some species, such as humans (Dostanic-Larson 2006). The α_4-isoform is expressed in sperm and is specifically synthetized at the spermatagonia stage, where it is required for sperm motility (Woo 2000).

It is reasonable to believe that the tissue-specific distribution of the α-isoforms indicates that each isoform exhibit a particular function associated with the tissue in which it is expressed.

Sodium pump probably plays a critical role during water absorption in the intestine and reabsorption in the kidney, because water and Na^+ transport across epithelia are invariably linked. So, sodium pump in kidney and small intestine can be associated with the pathophysiology of hypertension and chronic diarhea, respectively (Therien and Blostein 2000).

In excitable tissues such as neurons and skeletal muscle, the sodium pump must reestablish the electrical potencial across the plasma membrane following excitation-induced depolarization. The skeletal muscles contain one of the largest pools of Na^+/K^+ pumps in the body, and therefore play a central role in the clearance of K^+ from the blood during exercise and in the ingestion or infusion of K^+. Thus, the downregulation of Na^+/K^+ pumps in skeletal muscle developing during K^+ deficiency gains particular importance because attempts to restore the K^+ stores by the administration of K^+ will be associated with an increased risk of the development of hyperkalemia and cardiac arrest (Clausen 1996).

The Na^+/K^+-ATPase also serves as the unique binding site for the cardiac glycosides, such as ouabain, digoxin, and digitoxin. Digoxin is currently used widely in the treatment of congestive heart failure (Kaplan 2005). Dostanic-Larson et al. (2006) demonstrated that the cardiac glycoside binding site of Na^+/K^+-ATPase plays an important physiological role in blood pressure regulation. Regulation of the sodium pump in cardiac muscle is critical to the myocardium, for determining the „set-point" for cardiac muscle contraction and the steady-state contraction of vascular smooth muscle (Therien and Blostein 2000).

The sodium pump, in turn, is the target of multiple regulatory mechanisms activated in response to changing cellular requirements.

1.3 Sanguinarine

Sanguinarine, a quaternary benzo[c]phenanthridine alkaloid (QBA), is present in the *Papaveraceae*, *Fumariaceae*, and *Rutaceae* families of plants. The main sources of sanguinarine are the plant species *Chelidonium majus*, *Macleaya cordata*, and *Sanguinaria canadensis*. Sanguinarine exhibits multiple biological effects, in particular antimicrobial and antiinflammatory activities for which it is used in dental hygiene products and feed additives (Walterová et al. 1995). QBA extract from S. canadensis (sanguinaria) and M. cordata (sanguiritrin) have been used in toothpastes and mouthwashes as antiplaque agents. Sanguiritrin has been applied as a veterinary preparation for mastoiditis in cows (Faddeeva and Beliaeva 1997). QBA in Sangrovit[®] improve animal performance by eliminating the need for including low levels of antibiotics in the feed, which may be associated with the risk of antibiotic resistance (Psotová et al. 2006).

From chemical point of view, QBAs interconvert between the cationic vs. neutral form (i.e. hydroxide adduct of pseudobase, Fig. 9). They penetrate across the cell membrane in the hydrophobic pseudobase form acting as pro-drugs and convert into active cationic form once inside the cell (Šimánek et al. 2003). Both charged and uncharged forms of these alkaloids (QBAs) exist in more or less comparable concentrations in aqueous solutions and in blood at physiological pH 7.4. Charged (iminium) form of sanguinarine has been indicated as the form reacting with nucleophiles including mercapto nucleophile. In contrast, the uncharged form of sanguinarine was indicated as the form, which interacts with albumin (Vespalec et al. 2003).
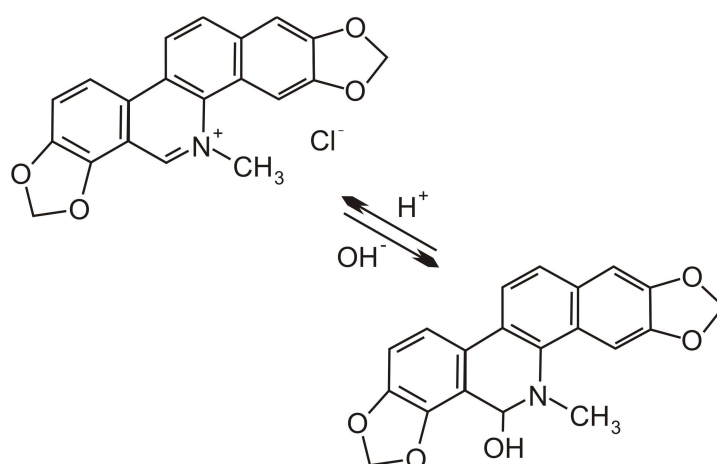
Figure 9 Scheme of conversion between quaternary cation (left) and pseudobase (right) form of sangunarine.

Due to the iminium bond, polycyclic and planar structure sanguinarine can react with nucleopholic and anionic moieties of amino acids in biomacromolecules (Schmeller et al. 1997). Futher, strong interaction to involve intercalation of sanguinarine into the adjacent basepair of the DNA has been described (Maiti et al. 1982).

The formation of DHSG (Fig. 10) might be the first step of SG detoxification in the organism (Psotová et al. 2005).
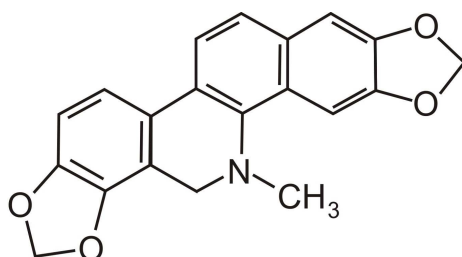
Figure 10 Structural formula of DHSG.

The Na^+/K^+-ATPase is suspected to be one of the targets of SG in cell. Unfortunately, the mechanisms of SG actions are poorly understood on the molecular level. Earlier studies reported that SG in the concentration range 5-20 μM inhibits Na^+/K^+-ATPase (Seifen et al. 1979; Straub and Carver 1975). On the other hand, enhanced cation flux was observed at higher SG concentrations (Moore and Rabovsky 1979; Nichols et al. 1978). Later, these apparently contradictory effects of SG on the sodium pump were explained by a proposal that the neutral form of SG (SGOH) can produce voltage-dependent channels in the lipid bilayer (Cala et al. 1982) or that SG forms a tight complex with Na^+/K^+-ATPase and converts it into a channel (Scheiner-Bobis 2001).

1.3.1. Photophysical and photochemical properties of sanguinarine

As was described previously, depending on the pH of the medium, the sanguinarine molecule can exist in two forms: the cationic and neutral form (i.e. hydroxide adduct of pseudobase, Fig. 9). Additionaly, it was shown that sanguinarine has also pH dependent spectral changes (Maiti et al. 1983). In the absorption spectra of a sanguinarine solution (pH 5.6), there are four bands with maxima at 275, 330, 396, and 471 nm, to which correspond $\pi \rightarrow \pi^*$ electronic transitions at 280, 323, 407, and 463 nm. In alkaline medium (pH 9.85), the absorption spectra of a sanguinarine solution have only two bands with maxima at 286 and 326 nm, to which

correspond $\pi \rightarrow \pi^*$ electronic transitions at 271 nm and 306 nm (Fig. 11) (Motevich et al. 2007). The short wavelenght absorption maximum at 275 nm shifted in alkaline medium to longer wavelenght (286 nm), and, moreover, the peak intensity at ~330 nm diminished with increasing pH (Maiti et al. 1983). The presence of two isobestic points at 286 and 307 nm in the pH dependent absorption spectra of sanguinarine (Fig. 11) confirmed a reversible equilibrium between cationic and pseudobase forms (Absolínová et al. 2009). Equilibrium constant of transition between pseudobase and cationic form of sanguinarine was determined with a pK value 7.5 (Maiti et al. 1983).
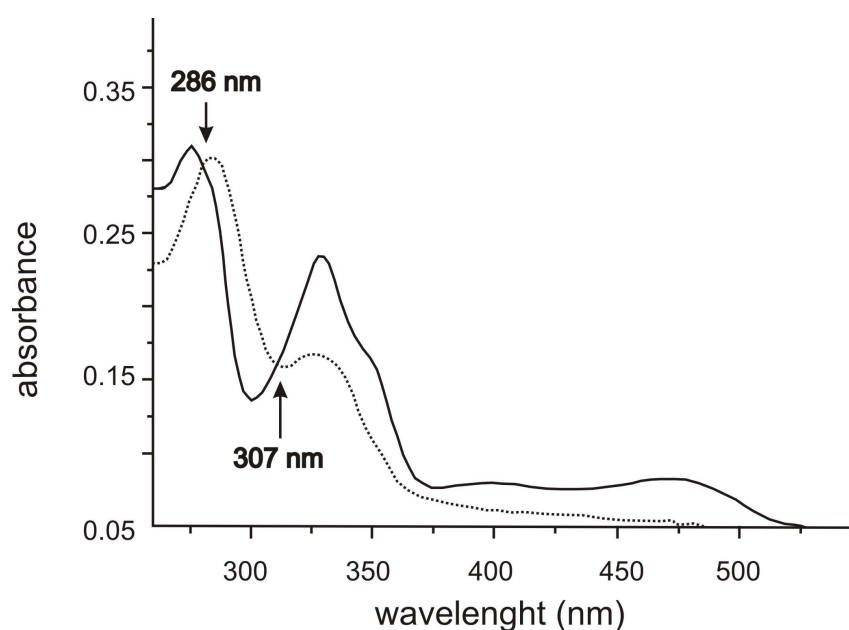
Figure 11 Absorption spectra of sanguinarine in aqueous solutions at pH 5.6 (solid line) and pH 9.85 (dashed line). Isobestic points at 286 and 307 nm are marked. Figure was adapted from Motevich et al. (2007).

It has been reported that fluorescence spectra of sanguinarine has two emission bands at 420 and 580 nm in water of pH 7.0, when excited at 329 nm. There is gradual attenuation of 580 nm band and increment of 418 nm band intensity with increase of pH and vice versa (Maiti et al. 1983). It was also reported that sanguinarine pseudobase form undergoes an irreversible photo-oxidation in the excited singlet state to produce oxysanguinarine (Kumar and Maiti 1997).

There were also provided absorption and fluorescence experiments with sanguinarine binding with the biomacromolecules. It was observed that binding of sanguinarine with the DNA

molecules has influence on spectral properties of sanguinarine. On addition of the DNA molecule to the alkaloid solution the absorption increase and the bands depose. Binding of sanguinarine to the DNA molecule has also influence on the excitation and emission fluorescence spectra of sanguinarine. The excitation spectrum shifts to the long-wave region on addition the DNA to the alkaloid solution. The emission intensity of the 420 nm maximum decreases by 1.5 times and shifts to the long-wave side too. As for maximum 580 nm – 3 times decrease and spectral shift to the long-wave side. It was shown that sanguinarine interacts with DNA by intercalation process and GC pairs binding (Bashmakova et al. 2008). Unfortunately, the interaction efficiency is lowered because of existing of the two forms of sanguinarine, quaternary cation and pseudobase form, while the pseudobase form of sanguinarine does not interacts with DNA (Maiti et al. 2002).

2 AIMS

The main aims of this thesis are:

    1) To study interactions of benzo[c]phenanthridine alkaloids with Na^+/K^+-ATPase.

    2) To study interactions of cytoplasmic ligands with Na^+/K^+-ATPase isolated large cytoplasmic loop.

3 MATERIALS AND METHODS

3.1 Reagents

Sanguinarine (13-Methyl-[1,3]benzodioxolo[5,6-c]-1,3-dioxolo[4,5-i]phenanthridinium chloride) and NADH were purchased from Sigma-Aldrich (Prague, Czech Republic). Dihydrosanguinarine (13,14-dihydro-13-methyl-[1,3]benzodioxolo[5,6-c]-1,3-dioxolo[4,5-i]phenanthridine, DHSG), 99 % purity, MP 189-191ºC was prepared from sanguinarine by reaction with $NaBH_4$ in methanol (Brossi and Borer 1965). Sanguinarine and dihydrosanguinarine were provided by V. Šimánek and J. Ulrichová.

Na^+/K^+-ATPase was supplied by Sigma and dissolved into 600 μl of sterilized 10 mM Tris-HCl, 100 mM NaCl, 10 mM KCl, pH 7.5 to 100 μM concentration. The ATPase stock solution was divided into aliquots and stored at -20°C.

Na^+/K^+-ATPase for activity measurements was purified from the pig kidney (Klodos et al. 2002) at the Department of Physiology and Biophysics, Aarhus University, Denmark. Kidney enzyme has a specific activity about 1500 - 1800 μmol Pi per mg protein per hour. The Na^+/K^+-ATPase accounts typically for 70% of the total protein (determined as the content of α- and β-subunits from SDS gel electrophoresis).

Samples for all fluorescence experiments were dissolved in 10 mM aqueous Tris buffer solution (Bio-Rad), pH 7.5, with four different proportions of NaCl (Fluka), KCl (Lachema), NaI (Sigma) and KI (Lachema). Proportions of salts in buffer for control experiments were 140 mM NaCl:10 mM KCl (NaCl-buffer) and 140 mM KCl:10 mM NaCl (KCl-buffer), and for quenching experiments were 140 mM NaI:10 mM KCl (NaI-buffer) and 140 mM KI:10 mM NaCl (KI-buffer). The pH value was set up by HCl (Lach-ner).

Effect of polarity on the fluorescence spectra of SG^+, SGOH and DHSG was evaluated in chloroform, butanol, acetone, ethyl alcohol, methanol, DMSO, 2-butanthiol, 1,2-ethanedithiol, and aqueous TRIS buffer solution, pH 7.5. All the solvents were from Sigma and were of spectrophotometric grade.

Neutral amino acid analogues Ac-Ser-OMe, Ac-Tyr-NH2, Ac-Glu-NH2, Ac-Gln-NH2, Ac-Lys-NH2.HCl, Ac-Arg-NH2-acetate salt, where Ac stands for acetyl and Me for methyl, were supplied by Bachem and Ac-Cys-OMe was supplied by Fluka.

3.2 Site-directed mutagenesis and fussion protein expression and purification

(site-directed mutagenesis was performed by L. Gryčová)

The native sequence of the C45 from the mouse brain Na$^+$/K$^+$-ATPase contains two Trp residues on the position 385 and 411. The cloning of the isolated C45, subsequent replacement of the two native tryptophans by phenylalanines (WT-W385F, WT-W411F, and WT-W385FW411F = TL; tryptophanless), insertion of the mutations TL-F404W, TL-F426W, TL-F571W, TL-I627W, TL-F683W, and TL-S732W into the tryptophanless construct yield the set of single tryptophan mutants (Fig. 12).
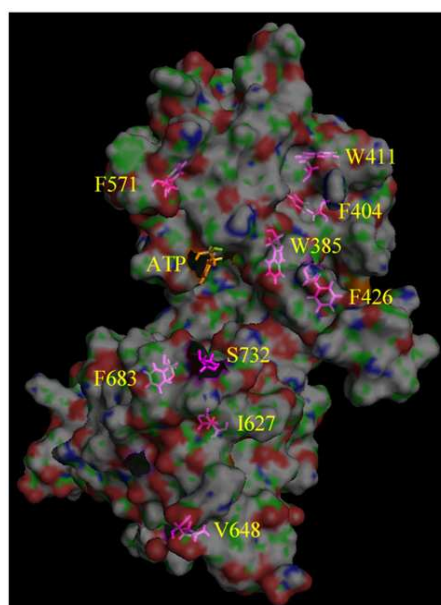
Figure 12 Positions of mutations on C45. Adapted from paper IV.

The DNA encoding C45 of the Na$^+$/K$^+$-ATPase and all its mutations were transformed into BL21 *Escherichia coli* bacteria (Promega) and were cultured at 37°C to OD(600 nm) of 0.6. Induction was carried out with 0.2mM IPTG (isopropyl β-D-thiogalactoside) overnight at 17°C. Cells were centrifuged at 5,000 g for 25 min, resuspended in 20 mM Tris–HCl, 140 mM NaCl, pH 7.4 containing protein inhibitors (2 μg/ml leupeptin, 2 μg/ml, pepstatin and 1 mM phenylmethylsulfonyl fluoride (PMSF)), disrupted by sonication and the homogenate was again centrifuged at 15,000 g for 25 min. All constructs were expressed as a (His)$_6$ – tag fusion protein; the (His)$_6$–tag was attached to the N-terminus. Purification by affinity chromatography was performed according to standard TALON Metal Affinity Resin

(Clontech) manufacturer protocol. The protein samples were eluted with 0.5 M Imidazol and were dialyzed against 1 liter of 50 mM Tris–HCl, 140 mM NaCl, pH 7.5 overnight at 4°C. The purity of protein samples was verified using 12% SDS-PAGE. Concentrations were estimated using the Bradford assay (Bradford 1976).

3.3 Tryptophan fluorescence quenching

The steady-state tryptophan fluorescence emission was quenched using 0-300 mM acrylamide (and/or KI for detection of changes in ESP, paper V) as a quencher. Data were collected using an excitation and emission wavelenghts of 295 nm and 360 nm, respectively, slits were set to 5 nm and 10 nm for the excitation and emission channel, respectively, the integration time was 3 s for recording of each point, the measurements were performed at 22°C. Protein samples were diluted to the final 3 µM concentration into 20 mM Tris-HCl, 140 mM NaCl, pH 7.5 buffer, where oxygen was removed by argon, and were titrated by aliquots of the quencher.

Quenching experiments were performed in four different setups i.e. without ligand, with 15 mM $MgCl_2$ (Lach-Ner), 15 mM Na_2ATP (Sigma) or 15 mM MgATP (Sigma). The experiments in the absence of magnesium were carried out in the presence of 5 mM EDTA. The efficiency of quenching was evaluated using the Stern-Volmer formula:

$$K_{SV} = \frac{\frac{F_0}{F} - 1}{[Q]}$$

where F_0 and F is the emission intensity in the absence or presence of quencher, respectively, *[Q]* is concentration of quencher and K_{SV} is Stern-Volmer quenching constant.

3.4 Time-resolved fluorescence measurements

(performed by M. Kubala)

Time-resolved fluorescence data were obtained by the time-correlated single photon counting (TCSPC) method on the PicoHarp300 instrument (PicoQuant, Berlin, Germany). The source of excitation pulses was pulsed LED centered at 298 nm (PLS300, PicoQuant) operating at 10

MHz frequency. The emission was sampled under magic-angle conditions through the monochromator set to 350 nm. The data were collected into the histogram spanning the 100 ns time-range with the 32 ps/channel resolution. The experiment proceeded until 10,000 counts in the peak channel were sampled. The instrument response function was measured using the colloid silica (Ludox, Sigma) as a scatterer. The *G*-factor was determined in the separate experiment.

Fluorescence decays were fitted using the FluoFit 4.2.1 software (PicoQuant) as a sum of exponencials with instrument response function (IRF) deconvolution:

$$I(t) = IRF \otimes \sum_i \alpha_i . e^{-t/\tau_i} ,$$

and the intensity-weighted mean fluorescence lifetime was calculated as

$$\tau_M = \frac{\sum \alpha_i \tau_i^2}{\sum \alpha_i \tau_i}.$$

Fluorescence anisotropy decays were fitted by the Pulse5Q software using the maximum entropy method (MEDC, Ltd.). Fluorescence anisotropy decays were analyzed as a sum of exponencials:

$$r(t) = \sum_i \beta_i \cdot e^{-t/\Phi_i} ,$$

where the set of the amplitudes β_i represents a distribution of the correlation times Φ_i. The β_i are related to the initial anisotropy r_0 by the formula:

$$\sum_i \beta_i = r_0.$$

All experiments were carried out at 20°C (bath-controlled).

3.5 Molecular dynamics modeling and simulations

(performed by P. Sklenovský and M. Otyepka)

At the beginning of the study, no experimentally determined structure of the entire Na$^+$/K$^+$-ATPase C45 was known. Therefore we created the C45 model in the closed conformation based on the homology with SERCA.

Molecular dynamic (MD) simulations have been performed with a homology model of the C45 with sodium or magnesium counterions in the absence of ATP (C45-Na and C45-Mg), as

well as with ATP bound to the active site of C45 (C45-Na$_2$ATP and C45-MgATP). Each system was immersed in a rectangular water box with a minimum distance between the molecule and the box wall of 9 Å. Experimental conditions are described in detail in the „Materials and methods" part of paper IV.

3.6 Electrostatic potential calculations

(performed by P. Sklenovský and M. Otyepka)

The electrostatic potential isocontour maps were calculated for the last snapshots of liganded and unliganded C45 MD simulations (C45-Na, C45-Na$_2$ATP, C45-Mg, and C45-MgATP) reported in Gryčová et al. (2009) using the program APBS (Baker et al. 2001) as implemented in the PMV software (Sanner 1999). The dielectric constants of the protein and the solvent were set to 2 and 78.5, respectively. The partial atomic charges for amino acid residues were assigned by AMBER force field of the PMV built-in PDB2PQR converter.

3.7 Excitation and emission spectra of SG and DHSG

The steady-state excitation and emission spectra of 10 μM SG or 5 μM DHSG were measured by a spectrofluorimeter F4500 (Hitachi, Japan). Data were collected with both excitation/emission bandpasses set to 10 nm. Scan speed was 240 nm/min. Excitation spectra were sampled with an emission wavelength 418 or 590 nm for SG, and 446 nm for DHSG. Emission spectra were sampled with excitation wavelengths 327 or 475 nm for SG, and 327 nm for DHSG. All measurements were performed at a temperature T=295 K, and in 10 mM Tris for UV spectroscopy (Fluka), pH 7.5 (except for some pH-dependence experiments - see below).

The spectra for measurement of solvent effects were measured in 100% solutions of chloroform, butanol, acetone, ethyl alcohol, methanol, DMSO, 1-butanethiol, 1,2-ethanedithiol and aqueous buffer solution (pH 7.5) and 10% solution of 1-butanethiol and 1,2-ethanedithiol in 20 mM Tris buffer, pH 7.5. Further, a 1 mM solution of the neutral analogs of amino acids Ser, Tyr, Glu, Gln, Lys, Arg and Cys in Tris buffer, pH 7.5 were used to test the influence of the functional groups found within proteins. The measurement was

performed in freshly prepared solutions of amino acid analogs. The experiment with Cys analog was done in a buffer that was deoxygenized by nitrogen to avoid oxidation.

Solvent effects are usually evaluated in the wavenumber scale. Therefore, the spectra were converted into the wavenumber scale using:

$$I(\nu) = I(\lambda).\lambda^2,$$

where λ is wavelength, ν is corresponding wavenumber and I is fluorescence intensity. The maximum of the peak ν_{max} was determined after smoothing by averaging over 10 adjacent points.

The solvent effects were evaluated by plotting of ν_{max} vs. ε_r (relative permittivity) or using the Lippert plot (ν_{ex}-ν_{em}) vs. Δf, where $\Delta f = (\varepsilon r-1)/(2\varepsilon r+1)-(n2-1)/(2n2+1)$., or the Kamlet-Taft solvatochromic analysis:

$$V = \nu_0 + a\alpha + b\beta + p\pi^*,$$

where V is the evaluated spectral characteristic (in our case ν_{ex}, ν_{em} or ν_{ex} - ν_{em}), ν_0, a, b, and p are the fitted parameters, the values of α (describing the ability of the solvent to donate a proton in a solute-to-solvent hydrogen bond), β (describing the ability of the solvent to accept a proton in a solute-to-solvent hydrogen bond), and π^* (which measures the ability of the solvent to stabilize a charge or a dipole by virtue of its dielectric effect) for individual solvents were taken from Kamlet et al. (1983).

After elimination of data revealing apparent specific reactivity between solvent and SGOH, SG^+ or DHSG, the remaining points in the graphs were fitted by linear function.

3.8 Dependence on pH

The influence of pH on SG and DHSG emission spectra was estimated in the pH range 5–12. Measurements were done in 10 mM buffers at pH 5, 6, 6.5 (MES, Sigma), 7, 7.5, 8, 8.5 (Tris, Fluka), 9, 9.5, 10, and 11 (CAPS, Sigma). Measurement at pH 12 was performed in 0.01 M NaOH solution. The final concentration of SG and DHSG in the sample was 5 and 2.5 µM, respectively. To estimate pK_a, dependence on relative fluorescence intensities F of SG on the pH at the excitation/emission wavelengths 327/418 nm or 475/590 nm was fitted to the following formula derived from the Henderson–Hasselbach equation:

$$F = F_B - \frac{F_B - F_A}{1 + 10^{pH - pK_a}},$$

where F_A and F_B represent fluorescence intensities of the acidic and basic forms, respectively.

3.9 Decay-associated spectra

(performed by M. Kubala)

Fluorescence decays of 20 μM solutions of SG or DHSG in the presence or absence of equimolar quantities of NADH were measured in 10 mM Tris, pH 7.5 on a TCSPC fluorimeter PicoHarp300 (Picoquant, Germany), using pulsed LED centered at 308 nm and operated at 10 MHz as the source of excitation light. Data were plotted as a histogram on a timescale of 0–100 ns, where the time-width of one channel was 32 ps. The instrument response function (IRF) was obtained using Ludox solution as a scatterer. FWHM was 0.45 ns. Emission wavelengths ranged from 360 to 690 nm with 10 nm steps. The emission bandpass was 16 nm. Data for each emission wavelength were acquired for 150 s, and about 1.2×10^7 photons were collected for each sample. The decay-associated spectra A_j (τ_j, λ_{em}) were recovered from the pre-exponential factors in the multiexponential global fit

$$I(t, \lambda_i) = IRF \otimes \sum_{j=1}^{n} A_j(\lambda_i) e^{-\frac{t}{\tau_j}}$$,

where the lifetime values τ_j were kept as global parameters (software FluoFit 4.2.1. , PicoQuant).

3.10 Fluorescence spectra of hepatocytes incubated with SG or DHSG

(hepatocytes were prepared by V. Šimánek and J. Ulrichová)

A liver sample was obtained from multi-organ donor. The tissue acquisition protocol was in accordance with Ethics Commission of the Faculty Hospital Olomouc. Hepatocytes were isolated according to a published protocol (Brossi and Borer 1965). They were suspended in serum-free ISOM's (Isom et al. 1985, Kosina et al. 2005) medium (20×10^6 cells/5 ml) with SG (1 μM) or DHSG (10 μM). The suspension was incubated at 37°C in a shaking water bath for 1 h. After incubation, the suspension was centrifuged at 2500 g/4°C for 10 min. The supernatant was frozen and stored at −80°C, and then the hepatocytes were twice rinsed with PBS medium, centrifuged, and stored at −80°C prior to analyses.

For the fluorescence measurements, the pelleted cells were resuspended in the buffer to $OD_{600}=0.05$ and fluorescence spectra of the suspension were sampled as described. Signals from cells that were not treated by SG or DHSG were subtracted as a background. Similarly for the supernatant fraction, the signal from the pure ISOM medium was subtracted as a background.

3.11 Determination of the dissociation constant from the steady-state fluorescence experiments

(performed by M. Kubala)

The steady-state SG and DHSG fluorescence emission spectra were measured on spectrofluorimeter F4500 (Hitachi, Japan). Slits were set to 10 nm for both the excitation and emission channel, respectively, scan speed was 240 nm/min, the measurements were performed at 22°C.

Increasing amounts of SG or DHSG were added to the NaCl- or KCl-buffer in the absence or presence of 5 μM Na^+/K^+-ATPase and the emission spectra were recorded after excitation at 327 nm (for monitoring of SGOH or DHSG binding) or at 475 nm (for monitoring of SG^+ binding). Then the plot of the normalized fluorescence intensity F (so that $F = 1$ for 1μM SG in the absence of protein) at the selected emission wavelength (see Results) on the SG concentration was fitted to the equation (Kubala et al. 2003):

$$F = [SG] + \frac{\gamma - 1}{2}\left([SG] + [E] + K_D - \sqrt{([SG]+[E]+K_D)^2 - 4[SG][E]}\right),$$

where *[SG]* and *[E]* represent the SG and enzyme concentration, respectively, K_D is the estimated dissociation constant and γ is the factor of relative fluorescence change upon binding (i.e. F_{bound}/F_{free}). Deviations of the experimental data from the fit were randomly distributed in all cases, indicating a correctness of the model used.

3.12 SG and DHSG fluorescence quenching

The steady-state SG$^+$, SGOH or DHSG fluorescence emission was monitored at the excitation/emission wavelengths 475/590 nm, 327/418 nm, and 327/446 nm, respectively, in the absence or presence of 5 μM Na$^+$/K$^+$-ATPase in NaCl-, KCl-, NaI- and KI-buffers, where the iodide anion served as a fluorescence quencher. Sample solution was titrated by aliquots of the sanguinarine resp. dihydrosanguinarine and the slopes from titration experiments were used for determination of quenching efficiency by Stern-Volmer formula:

$$K_{SV} = \frac{\frac{F_0}{F} - 1}{[Q]} \text{ ,}$$

where F_0 and F is the emission intensity in the absence (NaCl- or KCl-buffer) or presence of quencher (NaI- or KI-buffer), respectively, *[Q]* is concentration of quencher and K_{SV} is Stern-Volmer quenching constant.

3.13 Inhibition of Na$^+$/K$^+$-ATPase activity

Na$^+$/K$^+$-ATPase activity refers to the rate of the ouabain-sensitive hydrolysis of ATP at 37°C under optimal conditions in the presence of 4 μg of protein per sample in the reaction medium containing 130 mM NaCl, 20 mM KCl, 4 mM MgCl$_2$, and 30 mM histidine (pH 7.4 at 37°C). Na$^+$/K$^+$-ATPase was pre-incubated on ice in the presence of different concentrations of SG (DHSG) in the reaction medium for 30 minutes, then for 90 s in the water bath at 37°C. The reaction was induced by addition of 3 mM ATP. After 5 minutes at 37°C the reaction was stopped by addition of 50% trichloracetic acid and the amount of inorganic phosphate released was evaluated spectrophotometrically (Fiske and Subbarow 1925). Specific Na$^+$/K$^+$-ATPase activity was calculated from the difference in the amount of inorganic phosphate released in the absence and in the presence of ouabain.

4 RESULTS AND DISCUSSIONS

4.1 Interaction of benzo[c]phenanthridine alkaloids with Na$^+$/K$^+$-ATPase

4.1.1 Fluorescence properties of SG and DHSG (paper I)

Excitation and emission spectra of sanguinarine at pH 7.5 are complex (Fig. 13). There are three peaks in excitation spectrum with maximum at 327 nm for emission 418 nm, 395 nm, and 475 nm for emission at 590 nm. The 395 nm band in the excitation spectrum results in an emission spectrum which has an identical shape to the obtained upon excitation at 475 nm, probably represents the excitation into the S_2 state of the latter form.

Based on the pH dependence fluorescence spectra of sanguinarine with isoemissive point at 538 nm (Fig. 14), the blue-shift spectra with excitation/emission wavelength 327/418 nm were assigned to the SGOH form, while red-shifted spectra with excitation/emission wavelength 475/590 nm represents SG$^+$ form.
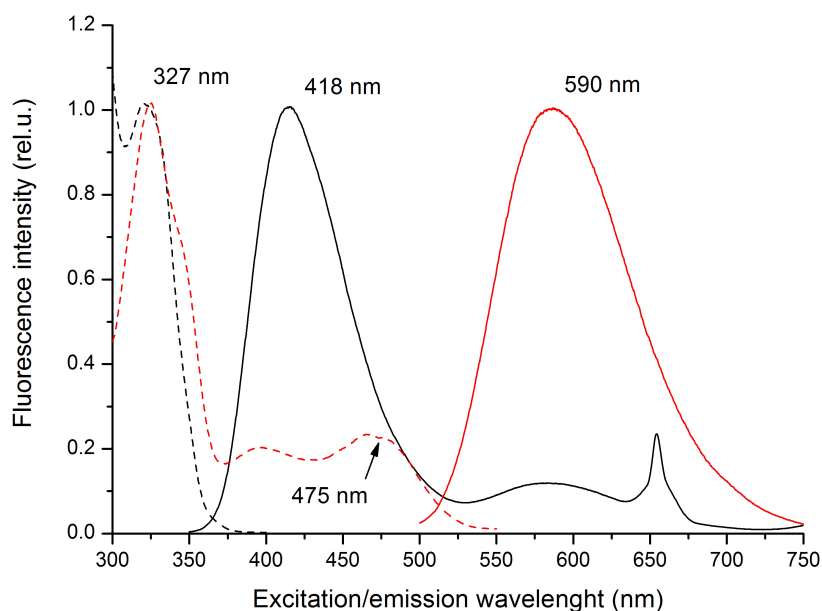
Figure 13 Excitation (dash lines) and emission (solid lines) spectra of SG. Spectra with excitation/emission wavelenght 327/418 and 475/590 nm are coloured black and red, respectively.
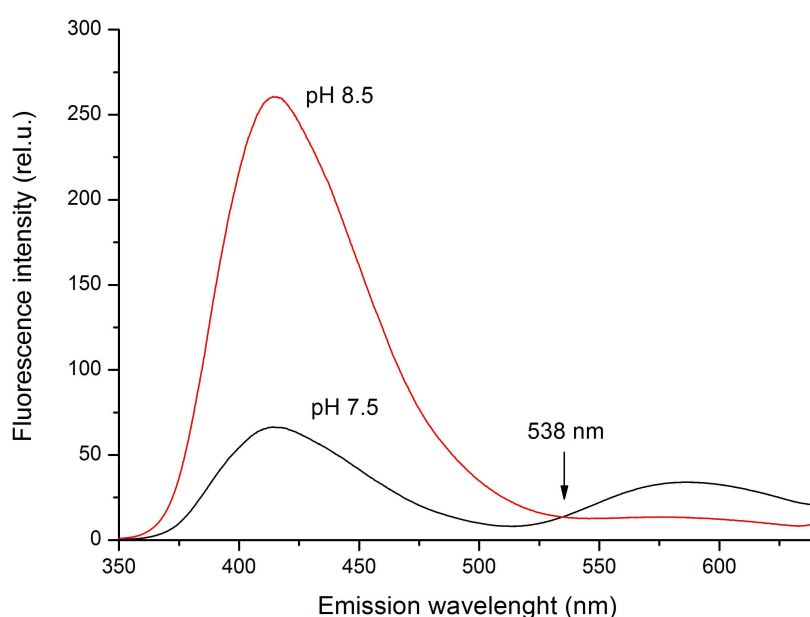
Figure 14 Emission spectra of SG upon excitation at 327 nm at solvents with various pH.

The pH dependence of spectra was also used for the calculation of acido-basic equilibrium constant. The sigmoidal curve (paper I, Fig. 4, on the right above) was fitted by equation given in the "Materials and methods" section and the fit yielded the pK_a = 8.06. This value is slightly different from the value pK_a = 7.5 yielded from the evaluation of changes in absorption spectra (Maiti et al. 1982), but better fits the values obtained by other methods (Walterová et al. 1980, Vlčková et al. 2004). Recent study revealed that these small discrepancies may be a consequence of different buffer composition (Absolínová et al. 2009). Time-resolved fluorescence experiments yielded excited-state lifetimes of 3.2 ns and 2.4 ns for SGOH and SG$^+$ form, respectively. Decay-associated spectra (DAS) of sanguinarine (paper I, Fig. 5a) were reconstructed from the dependence of pre-exponential factors on the emission wavelength. The addition of equimolar amount of NADH, which is naturally present in the cytoplasm, affected the DAS characteristics, and they fit well to the values estimated for DHSG (paper I, Fig. 5b) (see below). Based on this experiment we can say that SG does interact with NADH, on the other hand, there is no evidence for the negatively charged form, which has been proposed by Matkar et al. (2008) as a result of interconversion of SG forms in the presence of NADH. However, if this negatively charged form of SG is not fluorescent, we are not able to detect it.

Excitation and emission spectra of DHSG at pH 7.5 are simple (Fig. 15). There is one strong excitation peak at 327 nm for emission at 446 nm. The pH dependence experiments revealed no sensitivity of DHSG to acidity of the solution in pH range 5 to 12.

Time-resolved fluorescence measurement of DHSG yielded double-exponential decay with excited-state lifetimes of 4.2 and 1.8 ns. Decay-associated spectra were also reconstructed in the case of DHSG (paper I, Fig. 5c), but there is no evidence for interaction in the presence of NADH. DAS characteristics in this case can be considered as a simple superposition of the DHSG and NADH (paper I, Fig. 5d).
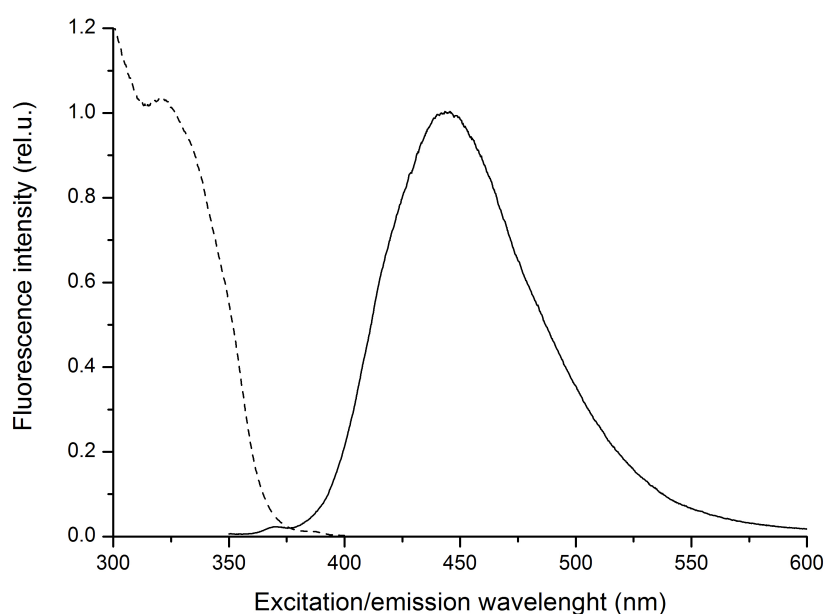
Figure 15 Excitation (dash line) and emission (solid line) spectra of dihydrosanguinarine.

One of the advantages of the fluorescence spectroscopy is that it is a non-invasive and non-destructive method, and hence, it can be used also for *in vivo* experiments. As mentioned above, experiments with SG are complicated by the fact, that SG is in the equilibrium between SGOH and SG$^+$ forms, and under physiological conditions, these two forms can never be separated. Moreover, *in vivo* SG can be metabolized to DHSG.

Assignment of the fluorescence characteristics to the various SG forms presented in this paragraph is fundamental for the future studies of SG biological interactions. It gives us a possibility to observe each SG form separately, without the need to separate the specie of interest physically.

4.1.2 SG-to-DHSG metabolization in hepatocytes (paper I)

SG was incubated with hepatocytes to test if our approach is applicable to cell culture experiments and to confirm if SG is transformed to DHSG as was described recently in the rat (Večeřa et al. 2007). The fluorescence spectra of SG were observed after 1h of incubation with hepatocytes and short centrifugation. Spectral properties of supernatant fraction upon excitation at 327 nm perfectly matched the DHSG spectrum with the single emission peak at 446 nm (paper I, Fig. 6). This observation proved the transformation of SG to DHSG. Pelleted fraction was resuspended in the ISOM medium. However, no fluorescence signal was detected in this pellet fraction. We can speculate that DHSG was transported out of the hepatocytes using a transport mechanism such as P-glycoprotein.

4.1.3 Spectral changes expected upon interactions of SG and DHSG with proteins (paper II)

Upon the SG/enzyme interaction two effects are expected to influence the fluorescence spectra. We evaulated general effect of the microenvironment polarity, which is expected to decrease, when SG is bound from the aqueous buffer to the binding pocket on the enzyme. Further, the spectra can be influenced by specific interactions with amino acids reactive groups. We demonstrate that precise analysis of fluorescence spectra can provide valuable information about the SG/enzyme interaction and we were able to identify the SG^+ binding site on the Na^+/K^+-ATPase.

4.1.3.1 Solvent effects

For the evaulation of solvent effect we used several approaches – solvent dependence of fluorescence spectra on permitivity (commonly used in e.g. potentiometry), Lippert plot (used in fluorescence spectroscopy) and the most general Kamlet-Taft analysis.

We observed anomalous behaviour of SGOH, SG^+ and DHSG spectra in 1, 2-ethanedithiol (paper II, Fig. 2, Fig. 3, and Fig. 4, respectively), and also of SGOH and SG^+ spectra in 1-butanethiol suggesting a specific interactions of all SG forms with –SH group. Therefore, these solvents were excluded from the analysis focused on the polarity effects.

Lippert plots revealed increasing Stokes-shift with increasing solvent polarizability in the case of SG^+ and DHSG (paper II, Fig. 5 and Table 1), which is typical for the $\pi \rightarrow \pi*$ transitions typical in the planar nitrogen-containing heterocycles. On the other hand, no clear trend was observed for SGOH. It is probably caused by involvement of $n \rightarrow \pi*$ transitions in some solvents, because the presence of the –OH group disturbs the planar shape of the aromatic system.

Detailed Kamlet-Taft multiparametric analysis of spectra (paper II, Table 2) revealed that the polarity effect is dominating only in the excitation spectrum of SG^+. The behaviour of fluorescence spectra of neutral form of sanguinarine (SGOH) and dihydrosanguinarine (DHSG) is also strongly influenced by ability of solvent to form solute-to-solvent hydrogen bonds.

4.1.3.2 Interactions with amino acids residues

For the testing specific interactions of SG^+, SGOH and DHSG with the amino acids we evaulated influence of neutral analogues containing all reactive groups that are found within amino acids, i. e. Cys (-SH), Ser (-OH), Glu (-COOH), Gln ($-CONH_2$), Lys (-NH2), Arg (-NH-C-$(NH_2)_2$) and Tyr as a representative of aromatic acid residues. The experiments with SG (and DHSG) and amino acids analogues were performed in aqueous buffer (which simulates alkaloid interactions on the protein surface) and in aprotic solvent – acetone (which simulates interactions in the hydrophobic binding pocket).

Only small spectral changes were observed for both forms of SG and DHSG in protic (aqueous) environment (Fig. 16, Fig. 17, and Fig. 18, respective). All these changes were observed in the presence of cysteinyl residue (accompanied by decrease in fluorescence intensity) and Glu and Tyr in the case of SG^+. On the other hand, large changes in fluorescence spectra were observed for both forms of SG in aprotic environment (acetone). There were shifts in the spectra of SGOH (Fig. 16) in the presence of Glu, Lys and Cys, and in the spectra of SG^+ (Fig. 17) in the presence of Arg and Glu. No changes in the presence of any amino acids analogues were observed in the spectra of DHSG in aprotic solvent (Fig. 18).
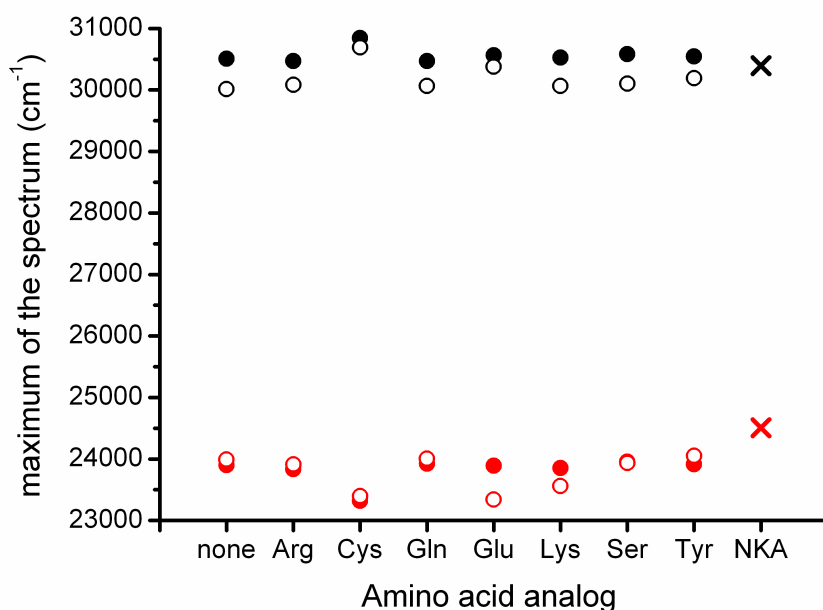
Figure 16 Sensitivity of the SGOH excitation (black) and emission (red) spectra to the presence of amino acid reactive groups in aqueous buffer (full symbols) and aceton (open symbols); NKA – interaction with Na^+/K^+-ATPase
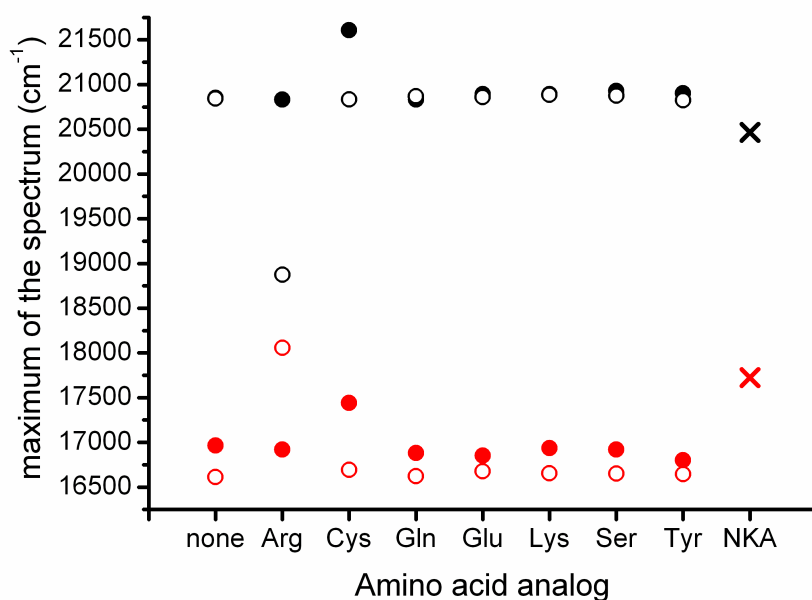
Figure 17 Sensitivity of the SG^+ excitation (black) and emission (red) spectra to the presence of amino acid reactive groups in aqueous buffer (full symbols) and aceton (open symbols); NKA – interaction with Na^+/K^+-ATPase
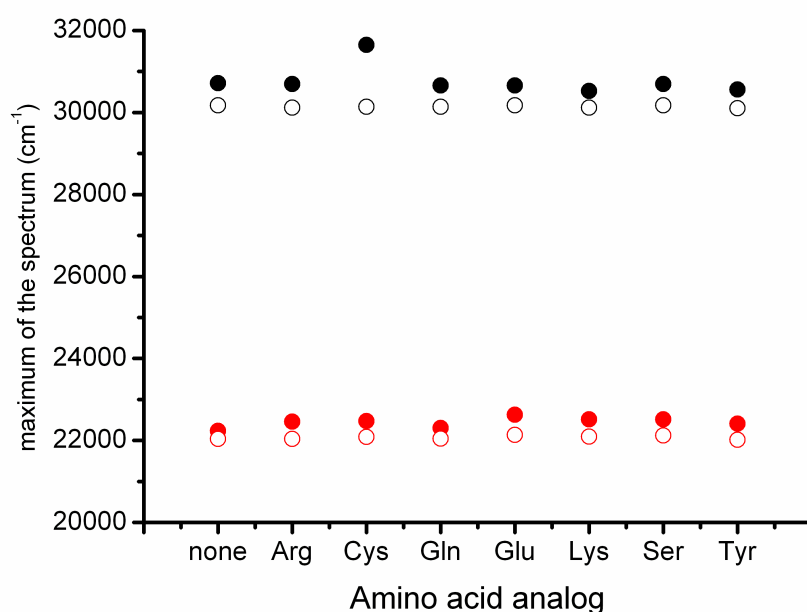
Figure 18 Sensitivity of the DHSG excitation (black) and emission (red) spectra to the presence of amino acid reactive groups in aqueous buffer (full symbols) and aceton (open symbols).

Up to now, the linkage between iminium bond of SG and free -SH group of cysteines was considered as the only mode of SG interaction with enzymes (Walterová et al. 1980, Vespalec et al. 2003). Our results unambigously demonstrated that in the aprotic environment we are able to detect interactions of both SGOH and SG$^+$ also with other amino acids.

4.1.3 Interactions of SG and DHSG with Na$^+$/K$^+$-ATPase (paper III)

Na$^+$/K$^+$- ATPase adopts two main conformational states during the catalytic cycle. There is E$_1$ state, with affinity for sodium, and E$_2$ state, with high affinity for potassium. E$_1$ state can be induced by the high concentration of sodium in the buffer solution, while E$_2$ conformation is obtained in the buffers with high potassium concentrations.

Structural details about interactions of alkaloids with Na$^+$/K$^+$-ATPase were evaulated on the basis of changes in fluorescence intensities, in excitation and emission spectra and from the fluorescence quenching experiments. The abovementioned spectral separation enabled individual monitoring of the SGOH, SG$^+$ or DHSG actions. The physiological effects of

alkaloid binding to the Na^+/K^+-ATPase were estimated from the ATPase activity measurements.

We observed quenching of SG^+ fluorescence and blue-shift of the SGOH fluorescence upon binding to Na^+/K^+-ATPase. Hence, fluorescence intensity changes at 590 nm for SG^+ or at 381 nm for SGOH were used for the calculation of K_D (paper III, Fig. 1). Calculated K_D value for the binding of SG^+ was 7.2 ± 2.0 μM, for binding of SGOH it was 11.7 ± 0.9 μM. In E_2 state, we observed binding of SG^+ with $K_D = 4.7 \pm 1.1$ μM, while no binding to E_2 state of Na^+/K^+-ATPase was observed for SGOH. According to our results, DHSG is not able to bind to any state of the enzyme. Predominant role of SG^+ in binding to Na^+/K^+-ATPase is in good agreement with the results of Cala et al. (1982).

The fluorescence quenching experiments provided some insight into the structural details of SG-binding site on Na^+/K^+-ATPase. We expected that effectivity of the collisional quenching is proportional to spatial accessibility of quencher to fluorophor. Small fluorophor (like SG or DHSG) bound to the protein is at least partialy protected from the solvent, thus, quencher has worse accessibility to fluorophor and quenching is less effective. Efficiency of quenching was analyzed by the evaulation of Stern-Volmer quenching constants (K_{sv}). Observed decrease in K_{sv} upon SG^+ or SGOH binding to E_1 state by a factor ~2 is typical for fluorophor that is located on the protein surface. It is not clear from our experiments, whether there are two binding sites for the SG^+ and SGOH or whether there is a single binding site for SG where the interconversion between SG^+ and SGOH is still possible by the proton exchange between SG and solvent.

The observed decrease in K_{sv} for SG^+ binding to E_2 state by a factor ~9 signifies that fluorophor is bound somewhere inside the hydrophobic binding pocket. This fits well to the observation that changes in SG^+ fluorescence spectra in the presence of Na^+/K^+-ATPase corresponds the best to changes in fluorescence spectra of SG^+ with Arg residue in aprotic environment. The high-resolution crystal structure of Na^+/K^+-ATPase (Morth et al. 2007, Shinoda et al. 2009) reveales that most of its arginine residues are located on the surface of the molecule, but only Arg^{979} on the α-subunit seems to be protected from the solvent (Fig. 19). Thus, we can conclude that Arg^{979} could be hot candidate for the interaction between SG^+ and Na^+/K^+-ATPase. Nevertheless, this is only hypothesis must be verified by future experiments.
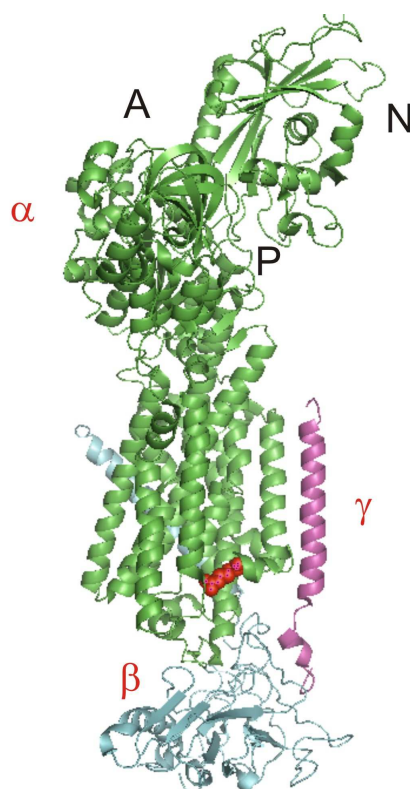
Figure 19 Localization of Arg^{979} (red spheres) within the $\alpha\beta\gamma$ complex of Na^+/K^+-ATPase in E_2 conformation (PDB entry 2ZXE). The α-, β-, and γ-subunits are colored green, blue and violet, respectively. Helices are represented by spirales and β-strands by arrows. Actuator, nucleotide binding, and phophorylation domains are labeled A, N, and P, respectively.

Results from ATPase activity measurement indicate that SG inhibits ATPase activity with IC_{50}=10.4 ± 2.2 µM (Fig. 20). This value corresponds well with the K_D values acquired from the steady-state fluorescence experiments. In opposite, no influence on ATPase activity was observed in the presence of DHSG.

In fact this negative result has very important consequences for the SG application in clinical praxis. Recalling the fact that SG is converted to DHSG in the gastro-intestinal tract implies that any biological effect that can be attributed to Na^+/K^+-ATPase inhibition by SG can be considered only prior to SG-to-DHSG metabolization in the living organism. Hence, it can be effective e.g. in the mouth-washes or cosmetic creams, but will be very limited after oral or parenteral administration.
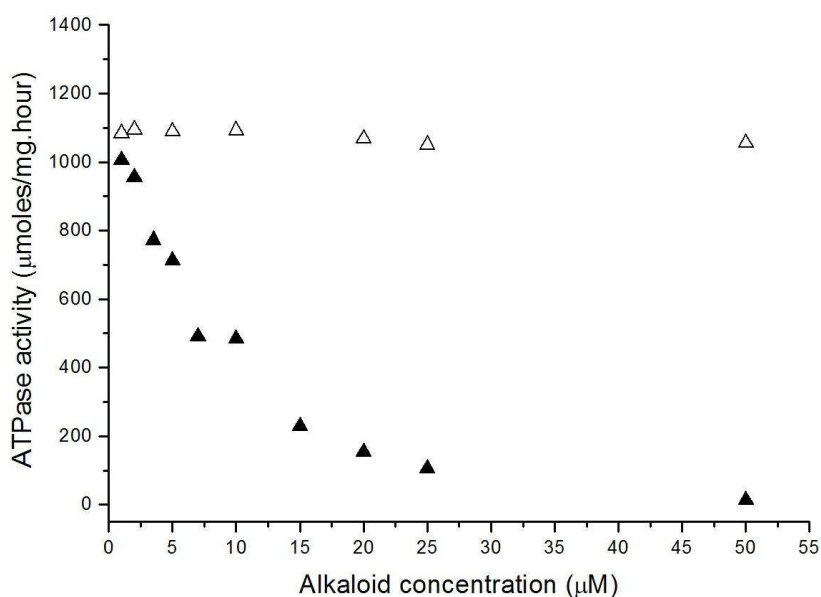
Figure 20 Effect of SG (solid symbols) and DHSG (open symbols) on the Na^+/K^+-ATPase activity.

4.2 Interactions of cytoplasmic ligands with Na^+/K^+-ATPase isolated large cytoplasmic loop C45

As was described above, Na^+/K^+-ATPase can exist in two conformational states during catalytic cycle. First, with high-affinity to ATP and sodium, generally known as E_1 state, second, with low-affinity to ATP and sodium, but high-affinity to potassium, generally known as E_2 state. Early experiments of Skou (1960) revealed that magnesium must be present in the cytoplasm as an essential cofactor that is not transported to the other side of the membrane. Pedersen et al. (2000) described location of the Mg^{2+}-binding site near the phosphorylation site and this fact lead to the consideration that only MgATP is the true ligand for P-type ATPases. It is generally agreed that magnesium is essential for the phosphorylation of the conserved Asp^{369}.

Recently published high-resolution crystallographic structures of Na^+/K^+-ATPase (Morth et al. 2007, Shinoda et al. 2009) provide detailed information about structure, but they represent only static pictures obtained under very extreme conditions and enzyme can be complexed only with molecules functioning as inhibitors. To observe the protein dynamics under

physiological conditions and with native ligands, the conventional spectroscopic techniques and molecular dynamic simulations are the better methods.

Our study introduced a novel approach for the observation of enzyme conformational changes upon binding of cytoplasmic ligands such Mg^{2+}, MgATP and ATP using the intrinsic tryptophan fluorescence quenching.

Cytoplasmic C45 loop containing the N- and P-domains constitutes ~40% of the α-subunit mass, and, as was described above, it could be isolated from the rest of the enzyme retaining its structure, as well as dynamic and some of its functional properties (e.g. TNP-ATP- or low-affinity ATP-binding).

The native C45 loop sequence contains two tryptophanyl residues (W385 and W411). They were subsequently replaced by phenylalanines to obtain a tryptophanless (TL) construct. Further, artificial reporter tryptophans were inserted into this TL construct to yield a set of single-tryptophan mutants (see Materials and methods, paper IV). Tryptophans were placed on the various positions on the C45 loop (Fig. 12). The expression levels of all mutants were high, suggesting that the carried out mutations did not influence the correct protein folding.

For the monitoring of enzyme conformational changes caused by the ligand binding, acrylamide quenching methods were used. The acrylamide quenching can reveal the information about the steric accessibility of the fluorofor. Additionaly, quenching by iodide was used for the monitoring of the local changes of the electrostatic surface potential (ESP) (Fig. 21).
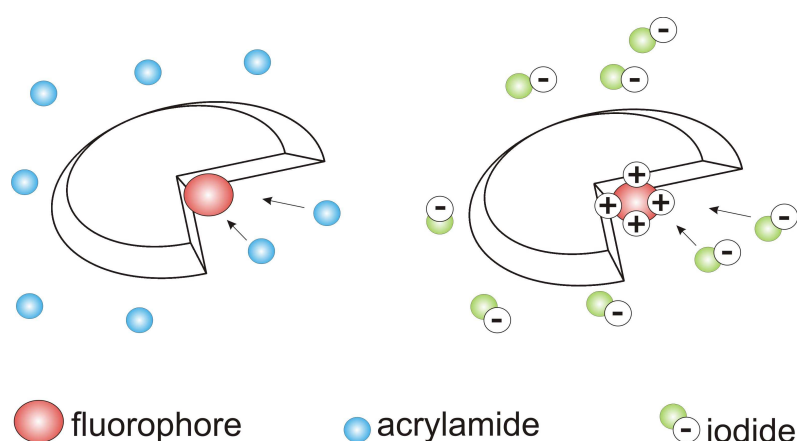
Figure 21 Scheme of fluorescence quenching by acrylamide and iodide. In the case of acrylamide, quenching effectivity depends mainly on the steric accessibility of the fluorophore. In the case of iodide, quenching effectivity depends also on the electrostatic interactions.

Observation of ESP was used for the better understanding of conformational events, because geometrical approach usually describes only the initial and final states. In opposite, ESP observation provides information about forces causing the movement. It is known that electrostatic forces play and important role in the inter- and intramolecular interactions.

4.2.1 Conformational changes caused by ligand-binding (paper IV)

Analyses of conformational changes caused by ligand-binding were accomplished using methods of intrinsic tryptophan fluorescence quenching by acrylamide, fluorescence anisotropy decay and molecular dynamic (MD) simulations. We can conclude, based on the C45-Xray MD simulation performed after remotion of C45 from the crystal structure of Na^+/K^+-ATPase that in the absence of any ligand C45 loop adopts closed conformation characteristic for the E_2 state.

In line with our expectation, binding of Mg^{2+} itself caused only slight changes and C45 still preserved the closed conformation. However, the largest changes were expected for binding of ATP in the presence of Mg^{2+}. In fact, the closed C45 structure changed only slightly, and, based on these results, we can conclude that MgATP stabilize closed C45 conformation. Moreover, our experiments suggested that there are two binding sites for Mg^{2+} in the proximity of the phosphorylation site. One of the cations was coordinated by the oxygens of the α- and β-phosphates, the other one was positioned between the γ-phosphate and phosphorylation site at Asp^{369}, with the assistance of the Val^{609} (paper IV, Fig. 5b).

The most dramatic changes were observed in the case of ATP binding in the absence of magnesium (Na₂ATP). ATP binding caused rapid opening of C45 conformation; the open C45 conformation is characteristic for E_1 state. Moreover, subsequent addition of Mg^{2+} caused C45 closure again (paper IV, Fig. 6). However, this conformation turned to be unstable (in the MD simulations) on longer time scale and we observed some kind of oscillations.

It is also important to note that there are some limitations related with the observation of conformational changes the C45 structure. Based on the crystal structure of SERCA, we suggest that the flanking stroke of A-domain into C45 is necessary to correct mutual orientation of the N- and P-domains. This could not have been observed in our studies with the isolated C45.

Based on our observations, we can conclude that conformational changes of C45 structure is dependent not on the binding of transported cations to the transmembrane domain but it depends on the presence or absence of the nucleotide and magnesium. It seems to be resonable to describe conformation of the cytoplasmic- and transmembrane domains within Albers-Post cycle independently. The proposed modification of the Albers-Post model based on our experiments is shown in Fig. 22 , where superscript "o" or "c" denotes the open or closed conformation of cytoplasmic headpiece and the subscript "Na" or "K" characterize high-affinity of the sodium or potassium ions to the transmembrane domain. First, ATP binds to the E_2 state of Na^+/K^+-ATPase with low-affinity for nucleotide. It causes opening of cytoplasmic headpiece conformation. This conformational change is transmitted to the transmembrane domain yielding change in affinities, from high-affinity for potassium to high-affinity for sodium, enzyme is in E_1 state. Cations can be exchanged on the cytoplasmic side. Then magnesium binds. It causes closure of the cytoplasmic headpiece, enabling the ATP hydrolysis and the enzyme phosphorylation. This is impulse for the transition from E_1 to E_2 conformational state of enzyme, thus, change in affinities for sodium and potassium. Potassium binding to the high-affinity E_2 state causes release of Mg^{2+} and enzyme is now ready for the binding another ATP molecule.

Our results correspond well with the fact that magnesium is necessary for the enzyme phosphorylation.
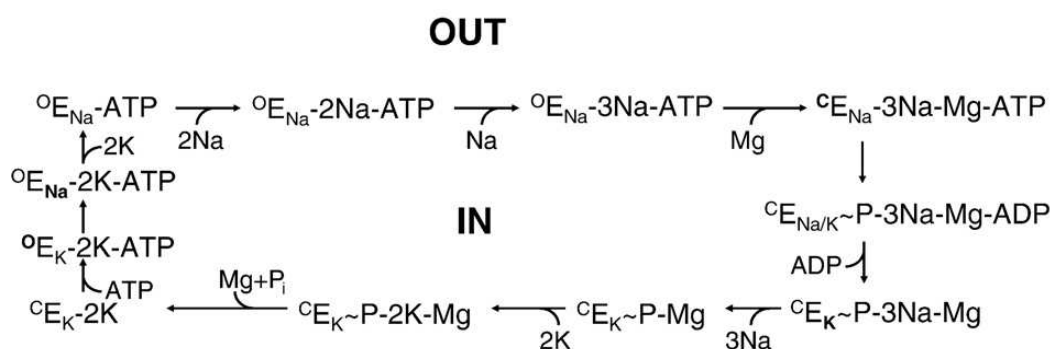
Figure 22 Proposed modification of the Albers-Post model based on our experiments. Adapted from paper IV.

4.1.3.2 Changes in electrostatic surface potential caused by ligand-binding (paper V)

It was described that transmembrane helices αM4, αM5, αM6 and αM8 of Na$^+$/K$^+$-ATPase participate to cation binding (Morth et al. 2007) and all 10 transmembrane helices are involved in complex structural changes (Toyoshima and Nomura 2002). In opposite, cytoplasmic segment C45 is the only interaction partner for external cofactors. It is interesting to know how the informations from the cytoplasmic headpiece can get to the transmembrane part of the enzyme. One of the possibilities is to study changes in electrostatic surface potential (ESP). We propose that changes in ESP could be important for the communication between distal parts of the molecule and can provide informations about the forces causing the movement, not only about the conformational changes from the point of view of the geometry.

In this study we introduced a novel approach to monitor the changes in electrostatic surface potential upon ligand-binding to C45 cytoplasmic segment. As was described above, for this study, we used the method of intrisic tryptophan fluorescence quenching by acrylamide and iodide, fluorescence decay measurement and the MD simulations.

Additionaly to the previous study, where the same set of single tryptophan mutants of C45 was used, the mutant TL-V648W exhibits upon ligand-binding a little changes in geometry but large changes in ESP. In opposite, other mutants, which were sensitive to the changes in geometry, did not show changes in ESP. Hence, the ESP mapping provides information that are complementary to the information obtained by evaluation of the conformational changes.

Based on the crystal structures of the calcium pump, it is obvious that large rearangement of the transmembrane helices occurs upon $E_1 \leftrightarrow E_2$ transition (Toyoshima and Nomura 2002). It is relatively straightforward to understand that the informations about nucleotide-binding can be transmitted to the transmembrane helices αM4 and αM5 of the enzyme, because they are extensions of C45, and that helices αM1-αM3 are influenced by the movement of A-domain. But it is not obvious how the information about nucleotide binding can get to the C-terminal transmembrane helices (αM7-αM10), which are located on the opposite the nucleotide-binding site.

According to our observations, local charge in the mutant V648W shifts toward more negative values in open conformation (induced by Na$_2$ATP binding) compared to the closed conformation. It could be signal for the short cytoplasmic loop C67, which was suggested (for example Xu et al. 2004), as a mediator of informations between C45 and C-terminal

transmembrane helices. Thus, our observations, based on the C45 MD simulations with the crystal structure of complete Na$^+$/K$^+$-ATPase, suggest that flexible loop Asn^{642}-Asn^{649} (paper V, Fig. 4 and Fig. S1) could mediate informations about nucleotide-binding between C45 loop and C-terminal transmembrane helices involving C67 short cytoplasmic loop as mediator.

Our data indicate that the effect of the ligand binding is not restricted only to the close environment of the binding site and that the information is in fact transmitted also to the distal parts of the molecule. This property could be important for the communication between the cytoplasmic headpiece and the cation binding sites located within the transmembrane domain. Moreover, our approach of ESP experimental monitoring opens a new way to understanding the interactions within the proteins.

5 CONCLUSIONS

Based on the work in this thesis, we conclude that:

- We have characterized fundamental fluorescence properties of SG+, SGOH, and DHSG. We found that inspite of the fact that, under physiological conditions, there is an equilibrium between quaternary cation (SG^+) and a pseudobase (SGOH) forms of SG and they can never be separated, we are able to observe them separately by the spectral selection.

- Acidobasic equilibrium constant characterizing transitions between SG^+ and SGOH is pK_a= 8.06. Fluorescence of DHSG exhibited no changes in the pH range 5-12.

- NADH is able to convert SG to DHSG, but there is no apparent interaction between NADH and DHSG.

- Our fluorescence experimental techniques are applicable for monitoring the SG to DHSG conversion in living cells.

- Fluorescence spectra of both forms of SG and to lesser extent also DHSG are sensitive to interactions that are predicted from binding to proteins.

- There are also other modes of SG interaction with proteins than the well known binding to cysteins.

- Hot candidate for the SG^+ binding site on Na^+/K^+-ATPase is Arg^{979}, which is, based on the recently published high-resolution crystal structure of Na^+/K^+-ATPase (Morth et al. 2007), in the protein structure protected from the solvent. This is also suggested by other fluorescence experiments in the presence of Na^+/K^+-ATPase, where the enzyme in E_2 conformation binds only SG^+ (not SGOH), while binding site is protected from the solvent. However, this hypothesis must be verified by further experiments.

- Enzyme in E_1 conformation can bind both charged (SG^+) and neutral (SGOH) form of SG and the binding site in E_1 conformation is located on the surface of the enzyme.

- There is no evidence for interaction of Na^+/K^+-ATPase and DHSG.

- Results from fluorescence experiments correspond well with the activity studies, where we observed inhibition of Na^+/K^+-ATPase activity by SG, but there was no effect on the enzyme activity in the presence of DHSG.

- Our interaction studies suggest that in vivo effect of SG attributable to inhibition of Na^+/K^+-ATPase can be considered only prior to SG→DHSG transformation in gastro-intestinal tract and/or blood. Hence, Na^+/K^+-ATPase inhibition will be effective in cosmetic preparations and mouth washes, but will be limited in duration in oral or parenteral administration.

- Our data from the intristic tryptophan fluorescence experiments with isolated large cytoplasmic loop of Na^+/K^+-ATPase (C45 loop) revealed that this model system consisting of only two domains retained the ability to adopt open or closed conformations induced by interactions with cytoplasmic ligands.

- The work with the isolated C45 loop enabled efficient separation of the events occurring within the transmembrane- and cytoplasmic parts of the Na^+/K^+-ATPase during the pumping cycle. We propose that free ATP is bound to the low-affinity binding site inducing opening of the cytoplasmic headpiece. Magnesium is bound later and induces closure of the cytoplasmic headpiece, thus enabling autophophorylation.

- We introduced the novel method for the monitoring of the changes in the electrostatic surface potential (ESP) induced by ligand binding, using the quenching of intritic tryptophan fluorescence.

- Our data from the monitoring of ESP indicate that the effect of the ligand binding is not restricted only to the close environment of the binding site and that the information is in fact transmitted also to the distal parts of the molecule.

6 REFERENCES

Absolínová H, Jančář L, Jančářová I, Vičar J, and Kubáň V (2009) Acid-base behaviour of sanguinarine and dihydrosanguinarine. *Ent. Eur. J. Chem. 7(4), 876-883*

Albers RW and Siegel GJ (1967) Sodium-potassium-activated adenosine triphosphatase of Electrophorus electric organ. *J. Biol. Chem. 242, 4972-4979*

Baker NA, Sept D, Joseph S, Holst MJ, and McCammon JA (2001) Electrostatics of nanosystems: application to microtubules and the ribosome. *Proc. Natl. Acad. Sci. USA 98, 10037-10041*

Bashmakova N, Hovorun D, Kutovyy S, Losytskyy M, and Yashchuk V (2008) The DNA influence on spectral properties of the berberine, chelidonine and sanguinarine alkaloids. *WDS´08 Proceedings of Contributed Papers, Part III, 163-167*

Beggah AT, Jaunin P, and Geering K (1997) Role of glycosylation and disulfide bond formation in the β-subunit in the folding and functional expression of Na,K-ATPase. *J. Biol. Chem. 272(15), 10318-10326*

Blanco G and Mercer RW (1998) Isozymes of the Na,K-ATPase heterogenity in structure, diversity in function. *Am. J. Physiol. Renal. Physiol. 275, F633-F650*

Bradford MM (1976) Rapid and sensitive method for quantitation of microgram quantities of protein utilizing principle of protein-dye binding. *Anal. Biochem. 72, 248–254*

Brossi A, Borer R (1965) Analysis and purification of a commercial sample of sanguinarine nitrate. *Lloydia 28, 199-&*

Cala PM, Norby JG, Tosteson DC (1982) Effects of the plant alkaloid sanguinarine on cation-transport by human red-blood-cells and lipid bilayer-membranes. *J. Membr. Biol. 64, 23-31*

Clausen T (1996) The Na^+,K^+ pump in skeletal muscle: quantification, regulation and functional significance. *Acta Physiol. Scand. 156, 227-235*

Das A, Nandi R, and Maiti M (1992) Photophysical property of sanguinarine in excited singlet state. *Photochem. Photobiol. 56(3), 311-317*

Dempski RE, Friedrich T, and Bamberg E (2005) The β-subunit of the Na^+/K^+-ATPase follows the conformational state of the holoenzyme. *J. Gen. Phys. 125, 505-520*

Dempski RE, Hartung K, Friedrich T, and Bamber E (2006) Fluorometric measurements of intermolecular distances between the Alpha and Beta subunits of the Na^+/K^+-ATPase. *J. Biol. Chem. 281(47), 36338-36346*

Dostanic-Larson I, Lorenz JN, Van Huysse JW, Neumann JC, Moseley AE, and Lingrel JB (2006) Physiological role of the $α_1$- and $α_2$-isoforms of the Na^+/K^+-ATPase and biological significance of their cardiac glycoside binding site. *Am. J. Physiol. Regul. Intel. Comp. Physiol. 290, R524-R528*

Emery AM, Billingsley PF, Ready PD, and Djamgoz MBA (1998) Insect Na^+/K^+-ATPase. J. *Insect Phys. 44, 197-209*

Ettrich R, Melicherčík M, Teisinger J, Ettrichová O, Krumscheid R, Hofbauerová K, Kvasnička P, Schoner W, and Amler E (2001) Three-dimensional structure of the large cytoplasmic H4-H5 loop of Na^+/K^+-ATPase deduced by restraint-based comparative modeling shows only one ATP binding site. *J. Mol. Model. 7, 184-192*

Faddeeva MD and Beliaeva TN (1997) Sanguinarine and ellipticine cytotoxic alkaloids isolated from well-known antitumor plants. Intracellular targets of their action. *Tsitologiia 39(2-3), 181-208*

Faddeeva MD, Beliaeva TN, and Sokolovskaia EL (1987) Effect of a number of biologically active substances on the activity of membrane-bound Na^+/K^+-ATPase from the bovine brain. *Tsitologiia 29(5), 576-581*

Fiske CH, Subbarow Y (1925) The colorimetric determination of phosphorus. *J. Biol. Chem. 66, 375-400*

Garty H and Karlish SJD (2006) Role of FXYD proteins in ion transport. *Annu. Rev. Physiol. 68, 431-459*

Gatto C, Wang AX, and Kaplan JH (1998) The C45 Cytoplasmic loop of the Na,K-ATPase, overexpressed in Escherichia coli, binds nucleoside triphosphates with the same selectivity as the intact native protein. *J. Biol. Chem. 273(17), 10578-10585*

Geering K (2001) The functional role of β-subunits in oligomeric P-type ATPases. *J. Bioenerg. Biomembr. 33, 425-438*

Geering K (2005) Function of FXYD proteins, regulators of Na,K-ATPase. *J. Bioenerg. Biomembr. 37(6), 387-392*

Geering K (2006) FXYD proteins: new regulators of Na, K-ATPase. *Am. J. Physiol. Renal. Physiol. 290, 241-250*

Girshin AV, Sverdlov VE, Kostina MB, Modyanov NN (1994) Cloning and characterization of the entire cDNA encoded by ATPAL1 – a member of the human Na,K/H,K-ATPase gene family. *FEBS Lett. 349, 144-150*

Hakim AH (1957) The use of the isolated perfused liver to detect alterations to plasma proteins. *Biochem. J. 66(2), 255-264*

Hu YK, Kaplan JH (2000) Expression of an active Na, K-ATPase with an alpha-subunit lacking all twenty-three native cysteine residues. *J. Biol. Chem. 275, 19185-19191*

Isom HC, Secott T, Georgoff I, Woodworth C, Mummaw J (1985) Maintenance of differentiated rat hepatocytes in primary culture. *Proc. Natl. Acad. Sci. USA 82(10), 3252–3256*

Jörgensen PL and Andersen JP (1988) Structural basis for E1-E2 conformational transitions in Na,K-pump and Ca-pump proteins. *J. Membr. Biol. 103, 95-120*

Jörgensen PL and Pedersen PA (2001) Structure-function relationships of Na^+, K^+, ATP, or Mg^{2+} binding and energy transduction in Na,K-ATPase. *Biochim. Biophys. Acta 1505, 57-74*

Jörgensen PL, Hakansson KO, and Karlish SJD (2003) Structure and mechanism of Na,K-ATPase: Functional Sites and Their Interactions. *Annu. Rev. Physiol. 65, 817-849*

Jörgensen PL, Jörgensen JR, and Pedersen PA (2001) Role of conserved TGDGVND-loop in Mg^{2+} binding, phosphorylation, and energy transfer in Na,K-ATPase. *J. Bioenerg. Biomembr. 33, 367-377*

Kamlet MJ, Abboud JLM, Abraham MH, and Taft RW (1983) Linear solvation energy relationships. 23. A comprehensive collection of the solvatochromic parameters, pi-star, alpha and beta, and some methods for simplifying the generalized solvatochromic equation. *J. Org. Chem. 48, 2877-2887*

Kaplan JH (2002) Biochemistry of Na,K-ATPase. *Annu. Rev. Biochem. 71, 511-535*

Kaplan JH (2005) The sodium pump and hypertension: A physiological role for the cardiac glycoside binding site of the Na,K-ATPase. *PNAS 102(44), 15723-15724*

Klodos I, Esmann M, Post RL (2002) Large-scale preparation of sodium-potassium ATPase from kidney outer medulla. *Kidney Int. 62, 2097-2100*

Köksoy AA (2002) Na^+/K^+-ATPase: A Review. *J. Ankara Med. Sch. 24 (2), 73-82*

Kosina P, Maurel P, Ulrichová J, Dvořák Z (2005) Effect of silybin and its glycosides on the expression of cytochromes p450 1A2 and 3A4 in primary cultures of human hepatocytes. *J. Biochem. Mol. Toxicol. 19(3), 149–153*

Kubala M, Hofbauerová K, Ettrich R, Kopecký Jr. V, Kumscheid R, Plášek J, Teisinger J, Schoner W, and Amler E (2002) Phe475 and Glu446 but not Ser445 participate in ATP-binding to the α-subunit of Na$^+$/K$^+$-ATPase. *Biochem. Biophys. Res. Com. 297. 154-159*

Kubala M, Plášek J, Amler E (2003) Limitations in linearized analyses of binding equilibria: binding of TNP-ATP to the H4-H5 loop of Na/K-ATPase. *Eur. Biophys. J. Biophys. Lett. 32, 363-369*

Kubala M, Teisinger J, Ettrich R, Hofbauerová K, Kopecký V, Baumruk V, Krumscheid R, Plášek J, Schroner W, and Amler E (2003b) Eight amino acids form the ATP recognition site of Na$^+$/K$^+$-ATPase. *Biochemistry 42(21), 6446-6452*

Kumar GS, Das A, and Maiti M (1997) Photochemical conversion of sanguinarine to oxysanguinarine. *J. Photochem. Photobiol. A: Chemistry 111, 51-56*

Laughery MD, Todd ML, and Kaplan JH (2003) Mutational analysis of α-β subunit interacions in the delivery of Na, K-ATPase heterodimers to the plasma membrane. *J. Biol. Chem. 278(37)34794-34803*

Lingrel JB, Kuntzweiler TJ (1994) Na$^+$,K$^+$-ATPase – Minireview. *Biol. Chem. 269, 19659-19662*

Lingrel JB, Williams MT, Vorhees CV, and Moseley AE (2007) Na, K-ATPase and the role of alpha isoforms in behaviour. *J. Bioenerg. Biomembr. 39, 385-389*

Linnertz H, Kost H, Obšil T, Kotyk A, Amler E, Schoner W (1998a) Erythrosin 5´-isothiocyanate labels Cys549 as part of the low-affinity ATP binding site of Na$^+$/K$^+$-ATPase. *FEBS Lett. 441, 103-105*

Linnertz H, Lanz E, Gregor M, Antolovič R, Krumscheid R, Obšil T, Slavík J, Kovařík Z, Schoner W, and Amler E (1999) Microenvironment of the high affinity ATP-binding site of Na$^+$/K$^+$-ATPase is slightly acidic. *Biochem. Biophys. Res. Com. 254, 215-221*

Linnertz H, Mikšík I, Kvasnička P, Bertoli E, Mazzanti L, Schoner W, and Amler E (1998b) Binding of pyrene isothiocyanate to the E1ATP site makes the H4-H5 cytoplasmic loop of Na$^+$/K$^+$-ATPase rigid. *Eur. J. Biochem. 251, 522-527*

Lutsenko S and Kaplan JH (1995) Organization of P-type ATPases: significance of structural diversity. *Biochemistry 34, 15607-15613*

Maiti M, Nandi R and Chaudhuri K (1982) Sanguinarine: a monofunctional intercalating alkaloid. *FEBS Lett. 142 (2), 280-284*

Maiti M, Nandi R, and Chaudhuri K (1983) The effect of pH on the absorption and fluorescence spectra of sanguinarine. *Photochem. Photobiol. 38, 245-249*

Maiti M, Das S, Sen A, Das A, Kumar GS, Nandi R (2002) Influence of DNA structures on the conversion of sanguinarine alkanolamine form to iminium form. *J. Biomol. Struct. Dyn. 20(3), 455-464*

Matkar S, Wrischnik L, Hellmann-Blumberg U (2008) Production of hydrogen peroxide and redox cycling can explain how sanguinarine and chelerythrine induce rapid apoptosis. *Arch. Biochem. Biophys. 477(1), 43-52*

Møller JV, Juul B, le Maire M (1996) Structural organization, ion transport, and energy transduction of P-type ATPases. *Biochim. Biophys. Acta 1286, 1-51*

Moore RD and Rabovsky JL (1979) Activation by sanguinarine of active sodium efflux from frog skeletal muscle in the presence of ouabain. *J. Physiol. 295, 1-20*

Morth JP, Pedersen BP, Toustrup-Jensen MS, Sorensen TLM, Petersen J, Andersen JP, Vilsen B, and Nissen P (2007) Crystal structure of the sodium-potassium pump. *Nature 450, 1043-1050*

Morth JP, Poulsen H, Toustrup-Jensen MS, Schack VR, Egebjerg J, Andersen JP, Vilsen B, and Nissen P (2009) The structure of the Na$^+$,K$^+$-ATPase and mapping of isoform differences and disease-related mutations. *Phil. Trans. R. Soc. B 364, 217-227*

Motevich IG, Strekal ND, Nowicky JW and Maskevich SA (2007) Absorption, fluorescence, and SERS spectra of sanguinarine in different pH values. *J. Applied Spectroscopy 74(5), 666-672*

Nichols J, Strub KD, Abernathy S (1978) Effect of sanguinarine, a benzophenanthridine alkaloid, on frog skin potential difference and short-circuit current. *Biochim. Biophys. Acta 511, 251-258*

Obšil T, Mérola F, Lewit-Bentley A, and Amler E (1998) The isolated H4-H5 loop of Na, K-ATPase overexpressed in Escherichia coli retains its ability to bind ATP. *FEBS Lett. 426, 297-300*

Palmgren MG, Axelsen KB (1998a) Evolution of P-type ATPases. *Biochim. Biophys. Acta 1365, 37-45*

Palmgren MG, Axelsen KB (1998b) Evolution of substrate specificities in the P-type ATPase superfamily. *J. Mol. Evol. 46, 84-101*

Pedersen PA, Jörgensen JR, and Jörgensen PL (2000) Importance of conserved α-subunit segment 709GDGVND for binding, phosphorylation, and energy transduction in Na, K-ATPase. *J. Biol. Chem. 275 (48), 37588-37595*

Pedersen PL, Carafoli E (1987a) Ion motive ATPases. I. Ubiquity, properties and significance to cell function. *Trends Biochem. Sciences 12, 146-150*

Pedersen PL, Carafoli E (1987b) Ion motive ATPases. II. Energy coupling and work output. *Trends Biochem. Sciences 12, 186-189*

Post RL, Hegyvary C, and Kume S (1972) Activation by adenosine triphosphate in the phospohorylation kinteics of sodium and potassium ion transport adenosine triphosphatase. *J. Biol. Chem. 247, 6530-6540*

Psotová J, Klejdus B, Večeřa R, Kosina P, Kubáň V, Vičar J, Šimánek V, and Ulrichová J (2005) A liquid chromatographic-mass spectrometric evidence of dihydrosanguinarine as a first metabolite of sanguinarine transformation in rat. *J. Chrom. B 830, 165-172*

Psotová J, Večeřa R, Zdařilová A, Anzenbacherová E, Kosina P, Svobodová A, Hrbáč J, Jirovský D, Stiborová M, Lichnovský V, Vicar J, Šimánek V, and Ulrichová J (2006) Safety assessment of sanguiritrin, alkaloid fraction of Macleaya cordata, in rats. *Veterinární Medicína 51(4), 145-155*

Sanner MF (1999) Python: a programming language for software integration and development. *J. Mol. Graph. 17, 57-61*

Seifen E, Adams RJ, and Riemer RK (1979) Sanguinarine: a positive inotropic alkaloid which inhibits cardiac Na^+/K^+-ATPase. *Eur. J. Pharmacol. 60(40), 373-377*

Shinoda T, Ogawa H, Cornelius F, and Toyoshima C (2009) Crystal structure of the sodium-potassium pump at 2.4 Å resolution. *Nature 459, 446-451*

Scheiner-Bobis G (2001) Sanguinarine induces K^+ outflow from yeast cells expressing mammalian sodium pumps. *Naunyn-Schmiedeberg´s Arch. Pharmacol. 363, 203-208*

Schmeller T, Latz-Brüning B, and Wink M (1997) Biochemical activities of berberine, palmatine and sanguinarine mediating chemical defence against microorganisms and herbivores. *Phytochem. 44(2), 257-266*

Skou JC (1960) Further investigation on a Mg^{++} + Na^+-activated adenosintriphosphatase, possibly related to the active, linked transport of Na^+ and K^+ across the nerve membrane. *Biochim. Biophys. Acta 42, 6-23*

Straub KD, Carver P (1975) Sanguinarine, inhibitor of Na-K dependent ATPase. *Biochem. Biophys. Res. Commun. 62, 913-922*

Sweadner KJ, Rael E (2000) The FXYD gene family of small ion transport regulators of channels: cDNA sequence, protein signature sequence, and expression. *Genomic 68, 41-56*

Šimánek V, Vespalec R, Šedo A, Ulrichová J, and Vičar J (2003) Quaternary benzo[c]phenanthridine alkaloids – biological activities. *Chem. Probes Biol., 245-254*

Therien AG and Blostein R (2000) Mechanisms of sodium pump regulation. *Am. J. Physiol. Cell Physiol. 279, C541-C566*

Toyoshima C, Nakasako M, Nomura H, and Ogawa H (2000) Crystal structure of the calcium pump of sarcoplasmic reticulum at 2.6 Å resolution. *Nature 405 (6787), 647-655*

Toyoshima C and Nomura H (2002) Structural changes in the calcium pump accompanying the dissociation of calcium. *Nature 418, 605-611*

Tran CM and Farley RA (1999) Catalytic activity of an isolated domain of Na,K-ATPase expressed in Escherichia coli. *Biophys. J. 77, 258-266*

Tsuda T, Shunji K, Funatsu H, Hayashi Y, and Taniguchi K (1998) Fluorescein 5´-isothiocyanate-modified Na$^+$,K$^+$-ATPase, at Lys-501 of the αchain, accepts ATP independent of pyridoxal 5´-diphospho-5´-adenosine modification at Lys-480. *J. Biochem. 123, 169-174*

Tyagarajan K, Chow DC, Smolka A, Forte JG (1995) Structural interactions between α- and β-subunits of the gastric H, K-ATPase. *Biochim. Biophys. Acta 1236, 105-113*

Vespalec R, Barták P, Šimánek V, Vlčková M (2003) Electrophoretic investigation of interactions of sanguinarine and chelerythrine with molecules containing mercapto group. *J. Chrom. B 797, 357-366*

Večeřa R, Klejdus B, Kosina P, Orolin J, Stiborová M, Smrček S, Vičar J, Dvořák Z, Ulrichová J, Kubáň V, Anzenbacher P, Šimánek V (2007) Disposition of sanguinarine in the rat. *Xenobiotika 37(5), 549-558*

Vlčková M, Barták P, Kubáň V (2004) Capillary electrophoretic studies of acido-base properties of sanguinarine and chelerythrine alkaloids. *J. Chromatogr. A. 1040(1), 141-145*

Walterová D, Preininger V, Grambal F, Šimánek V, Šantavý F (1980) On isolation and chemistry of alkaloids from some plants of the family Papaveraccae. 78. Fluorescence-spectra and cation-pseudobase equilibria of some benzophenanthridine alkaloids. *Heterocycles 14(5), 597-600*

Walterová D, Ulrichová J, Valka I et al. (1995) Cytotoxicity of benzo[c]phenanthridinium in isolated rat hepatocytes. *Acta. Univ. Palacki. Olomouc. Fac. Med. 139, 7-16*

Woo AL, James PF, and Lingrel JB (2000) Sperm motility is dependent on a unique isoform of the Na,K-ATPase. *J. Biol. Chem. 275, 20693-20699*

Xu C, Rice WJ, Wanzhong H, and Stokes DL (2002) A structural model for the catalytic cycle of Ca^{2+}-ATPase. *J. Mol. Biol. 316, 201-211*

Xu GY, Kane DJ, Faller LD, and Farley FA (2004) The role of loop 6/7 in folding and functional performance of Na,K-ATPase. *J. Biol. Chem. 279, 4594-45602*

Xu KY (2005) Activation of $(Na^+ + K^+)$ - ATPase. *Biochem. Biophys. Res. Comm. 338, 1669-1667*